Master's Theses   Master's Theses and Graduate Research

1996

Calculations and measurements of neutron arrival time for neutron detectors at SLAC

Kaur Rupinder
San Jose State University

Follow this and additional works at: https://scholarworks.sjsu.edu/etd_theses

INFORMATION TO USERS

This manuscript has been reproduced from the microfilm master. UMI films the text directly from the original or copy submitted. Thus, some thesis and dissertation copies are in typewriter face, while others may be from any type of computer printer.

The quality of this reproduction is dependent upon the quality of the copy submitted. Broken or indistinct print, colored or poor quality illustrations and photographs, print bleedthrough, substandard margins, and improper alignment can adversely affect reproduction.

In the unlikely event that the author did not send UMI a complete manuscript and there are missing pages, these will be noted. Also, if unauthorized copyright material had to be removed, a note will indicate the deletion.

Oversize materials (e.g., maps, drawings, charts) are reproduced by sectioning the original, beginning at the upper left-hand corner and continuing from left to right in equal sections with small overlaps. Each original is also photographed in one exposure and is included in reduced form at the back of the book.

Photographs included in the original manuscript have been reproduced xerographically in this copy. Higher quality 6" x 9" black and white photographic prints are available for any photographs or illustrations appearing in this copy for an additional charge. Contact UMI directly to order.

CALCULATIONS AND MEASUREMENTS OF NEUTRON ARRIVAL TIME FOR

NEUTRON DETECTORS AT SLAC

A Thesis

Presented to

The Faculty of the Nuclear Science Program

San Jose State University

In Partial Fulfillment

of the Requirements for the Degree

Master of Science

by

Rupinder Kaur

August 1996

UMI Number: 1381424

UMI
300 North Zeeb Road
Ann Arbor, MI 48103

APPROVED FOR THE DEPARTMENT OF NUCLEAR SCIENCE

_____

Dr. Allen B. Tucker

_____

Dr. James C. Liu

_____

Dr. Sayed H Rokni

_____

Dr. Vashek Vylet

_____

Dr. Herbert B. Silber

APPROVED FOR THE UNIVERSITY

_____

ABSTRACT

CALCULATIONS AND MEASUREMENTS OF NEUTRON ARRIVAL TIME FOR NEUTRON DETECTORS AT SLAC.

by Rupinder Kaur

The distributions of neutron arrival time (the time between the neutron being generated in a target and the time it is detected by the sensor) are important for the dead time corrections of the neutron detectors in pulsed radiation field. Calculations using MCNP and measurements of the neutron arrival time distributions were made for the moderated BF_3 detector, Anderson-Braun remmeter, and Bonner Sphere LiI detectors. Neutron sources defined in these calculations include monoenergetic neutrons from a few eV to 20 MeV, giant resonance neutrons, and the measured 'equilibrium' neutron spectrum of Final Focus Test Beam (FFTB) at SLAC. The results show an exponential behavior of the neutron arrival time distributions. Comparisons between calculations and measurements show close agreement for 10″ Bonner Sphere detector and a maximum difference of about 20% for moderated BF_3 detector and AB remmeter. The cause of the discrepancy for 2″ Bonner Sphere detector is also explained.

ACKNOWLEDGMENTS

I would like to thank Dr. J. C. Liu of SLAC for giving me the opportunity to work on this project. I greatly appreciate his supervision, guidance and deep involvement in this work. I am thankful to Dr. Allen B. Tucker and Dr. Herbert B. Silber of SJSU for reviewing and approving my work. Thanks are also due to all thesis committee members for their helpful reviews.

Special thanks go to Dr. Sayed H Rokni of SLAC for his help in measurement portion and to Dr. Vashek Vylet of SLAC for the valuable discussions on many aspects throughout this work. I would also like to thank Mr. Ron Seefred of SLAC for his help in the electronics set up.

I express my indebtedness to my parents for their support and efforts in all the accomplishments of my life. I am extremely grateful to my husband Sukhdev Singh for his never-ending encouragement, understanding, support, love and care. This thesis is dedicated to my family.

TABLE OF CONTENTS

APPENDICES

LIST OF TABLES

LIST OF FIGURES

1. INTRODUCTION

1.1 Introduction

Neutrons, being neutral particles, can be detected only through nuclear reactions that convert them to energetic charged particles such as protons or alpha particles. Any neutron detector, therefore, would include: a material for this conversion and a charged particle detector. Detection of neutrons imposes a great challenge for various reasons. Typical neutron fields span many decades of energy (0.1 eV to 1 GeV). For the reactions of interest, the neutron cross section depends strongly on neutron energy. For example, the thermal neutron (0.025 eV) cross section for $^{10}B(n, \alpha)^7Li$ is 3840 barns. The cross section value drops rapidly with increasing neutron energy and it is proportional to the reciprocal of neutron velocity (1/v). At 1 MeV neutron energy, the cross section for this reaction reduces to a mere 0.2 barns (Knoll 1989). Various detection technologies have been developed in different neutron energy regions.

Slow neutrons (below about 0.5 eV) are relatively simple to detect by neutron capture in some materials due to their large cross section. Fast neutrons may be detected by slowing them down using a moderator before they reach the thermal neutron sensor. The process in which a fast neutron loses most of its initial kinetic energy (in a series of elastic collisions) to become thermal neutron is called 'moderation.' This can be best achieved by using hydrogenous materials such as polyethylene and paraffin. Hydrogen is a very suitable moderator since it can absorb the largest fraction* of neutron energy per elastic

---

* In particular, for hydrogen scattering, the average energy loss is one half of the initial neutron energy.

1

collision. A thermal neutron detector is surrounded by a moderator to form a fast neutron detector. Examples of such moderator type detectors include an Anderson-Braun (AB) remmeter and Bonner Sphere detectors.

For most applications, the detectors are operated in pulse mode*. Any detector system operated in pulse mode has some dead time in which there is always some probability that the true event will be lost. The dead time of BF_3-based counters is a few μs. Therefore, the data analysis must include a dead time correction factor to get an accurate count rate.

In a pulsed radiation field such as that in an accelerator facility like Stanford Linear Accelerator Center (SLAC), the radiation measurements can also be affected by the duty factor* of the beam. The more seriously affected instruments include GM counters, proportional counters, bare BF_3 counters and scintillation counters. The detectors with moderators are less prone to this effect, because the signal is delayed by the long neutron arrival time (several hundreds of μs). The arrival time of neutrons in such detectors does affect the dead time correction factor.

1.2 Dead Time Correction

To compensate for the loss of counts due to the dead time of the detector, a correction factor must be incorporated in the measured count rate. Two models for the dead time behavior of a counting system have been in use; paralyzable model and non-paralyzable

---

* In pulse mode operation, the measurement instrumentation is designed to record each individual quantum of radiation that interacts in the detector.

* Duty factor is defined as the fraction of time during which an accelerator delivers a useful beam.

2

model (Knoll 1989). In the paralyzable model, the dead periods are not always of fixed

length. The true counting rate R_t is calculated as:

$$R_t = R \, e^{-RT_d}$$ (1)

where R = measured counting rate and T_d = dead time of the detector.

In the non-paralyzable model, a fixed dead time T_d is assumed and the true counting

rate R_t is calculated as:

$$R_t = \frac{R}{1 - RT_d}$$ (2)

These models represent an idealized behavior. Either of these may resemble the response

of a real counting system. Equations (1) and (2) assume that the detector is being

irradiated from a continuos radiation source. If the field is pulsed (i.e., short pulses

repeated at a constant frequency), the appropriate correction depends on the relative value

of the detector dead time T_d and the beam pulse length T_p. For most accelerator beams

($T_p \approx 1$ μs) and most health physics neutron instruments ($T_d \approx$ a few μs) where $T_p < T_d$,

the following equation should be used (Liu 1991):

$$R_t = R - P \ln\left(1 - \frac{R}{P}\right)$$ (3)

where P = pulse repetition rate.

If $T_p > T_d$, then the following equation should be used (Liu 1991):

$$R_t = \frac{R}{1 - \frac{RT_d}{PT_p}(1 - \frac{1}{2}\frac{T_d}{T_p})} \qquad (4)$$

where PT_p = duty factor.

In situations where moderating type detectors are used for detecting pulsed neutron fields, equation (3) is not valid. Due to moderation and diffusion, short pulses of neutrons (smaller T_p) are stretched over a longer period of time called the neutron arrival time, which could be a few hundreds of microseconds ($T_p > >T_d$). Therefore, equation (4) should be used. In this study, the arrival time of a neutron has been defined as the time between the neutron incident on the surface of the detector and the neutron detected by the sensor. It is the sum of the moderation time* and the diffusion time†. The neutron arrival time is generally dominated by the diffusion time. The signal recorded by the thermal neutron sensor is delayed with respect to the beam pulse. Therefore, effective beam pulse length in equation (4) should not be determined only by the physical T_p value. In this case, T_p is replaced with T_m (mean arrival time) and since $T_m >> T_d$, the

---

* The time for a fast neutron to slow down in the moderator to become a thermal neutron.

† The time for a thermal neutron to diffuse in the moderator and reach the sensor.

4

parenthetical term in equation (4) is neglected with small error. The equation (4) then

becomes equation (5):

$$R_c = \frac{R}{1 - \dfrac{RT_d}{PT_m}} \qquad (5)$$

It is assumed in equation (5) that the detected neutrons are uniformly distributed in

time T_m. T_m is called the mean moderation time by Jenkins (1979). In fact, T_m should be

referred to the mean arrival time as the delay of the signal is caused by both moderation

and diffusion. In this study, T_m is called the mean arrival time or the T-values.

According to measurements (Ash 1977), the neutron arrival time distribution is close

to an exponential distribution. Therefore, the inverse of the slope of the arrival time

distribution curve is the mean arrival time T_m. By incorporating this fact in equation (5)

for paralyzable model, the true count rate can be calculated as follows (Liu 1991):

$$R_c = Rr\ln\frac{r}{r-1} \qquad (6)$$

$$\text{where} \quad r = \frac{PT_m}{RT_d}$$

The parameter r is the ratio of maximum counting rate that can be measured (PT_m / T_d) to the measured counting rate (R).

The spread of the signal due to moderation and diffusion has made the measurements of neutrons less prone to the dead time losses in pulsed fields. In the absence of moderator, the detector would utmost record a single signal pulse per beam pulse. The dramatic influence of the moderator on the dead time correction is illustrated by the following example. For a proton recoil counter, at a pulse repetition rate of 10 Hz, a correction factor is about 1.5 at a measured counting rate of only 2 counts/sec. On the other hand, for the moderated BF_3 detector surrounded by 6.3 cm of paraffin, a correction factor of 1.5 is required for a high count rate of ≈ 500 counts/sec at 10 Hz (Patterson 1973).

1.3 Neutron Production at SLAC

SLAC has a two-mile-long linear accelerator that accelerates electron and positron beams up to an energy of 50 GeV. These beams can be sent to different experimental facilities. One of such facilities is the Final Focus Test Beam (FFTB). The measurements for the present work have been made outside the shielding of the FFTB beam dump.

When a very high energy electron beam interacts with matter, only a small fraction of energy is dissipated through heat or ionization. The large fraction of the energy is spent in the production of high energy photons by bremsstrahlung. The fraction of the kinetic energy of the incident electrons converted to bremsstrahlung is a function of incident

electron energy (E_o) that increases with the increasing E_o. The bremsstrahlung photons, in

turn, can undergo pair production to produce electron and positron pairs or compton

collisions to produce electrons. These new secondary electrons and positrons radiate even

more photons and the process goes on until eventually the energies of particles become

low. This process is known as electromagnetic (EM) shower.

Neutrons are produced in any material struck by the electron or bremsstrahlung beams

of energies above a certain threshold (for example, 4 to 6 MeV for heavy nuclei). It is the

photons that release the neutrons by photonuclear reactions rather than the direct

interaction of electrons. The mechanisms by which neutrons are produced are as follows

(IAEA 1979):

Giant resonance

For photon energy above a certain threshold and below 30 MeV, neutron production

results primarily from a process known as giant resonance. The electric field of a

photon transfers its energy to nucleus by inducing an oscillation in which protons as a

group moves opposite to the neutrons as a group. Neutrons emitted in the decay of

this nuclear excitation are called Giant Resonance Neutrons (GRN). The average

energy of GRN is in the order of a few MeVs.

Pseudo-deuteron

At photon energies above 30 MeV and below 100 MeV, neutrons are produced by

pseudo-deuteron mechanism. In this neutron production mechanism, photo-

disintegration of nucleon pairs within the nucleus takes place. Pseudo-deuterons are

7

more energetic than GRNs. The cross section for this mechanism is an order of magnitude lower than the GRN peak.

Photopion

Photons of energy above the pion threshold (140 MeV) produce neutrons by photopion reaction. These neutrons are much higher in energy than those from GRN and pseudo deuterons. The cross section goes through a number of resonance peaks. At very high energy electron accelerators, these neutrons make the dominant contribution to the dose rate outside the massive concrete shielding. Only the neutrons with the highest energies are able to penetrate through the thick shielding. The lower energy portions of neutron spectra outside the shielding are generated by these high energy neutrons interacting in the outer layers of the shielding.

1.4 Objective

The objective of this work was to calculate the neutron arrival time distributions for common neutron detectors and compare the results with the measurements made outside the shielding of the FFTB beam dump. The T-values for FFTB spectrum have also been estimated for various neutron detectors from their calculated neutron arrival time distributions. The detectors used for this study were a moderated BF_3 counter, an AB remmeter, and Bonner Sphere detectors (LiI sensor) of 2", 3", 5", 8", 10", and 12" diameter.

The neutron arrival time distribution is a differential plot of the number of neutrons detected by the sensor versus their corresponding arrival time. In the moderating type detectors, there can be a substantial delay for neutrons to be detected after their incidence on the detector surface. The delay depends on the thickness of the moderator. The significant time delay does not result from the slowing down of the neutrons to thermal energies, but from the diffusion of the thermal neutrons in the moderator.

The investigation of the timing effect of the moderator thickness on the arrival of the neutrons is the primary focus of this study. The neutron arrival time distributions along with the energy response of the various detectors have been calculated using the MCNP4A Monte Carlo code (MCNP 1993). Measurements have been performed with four detectors to record the number and arrival time of the neutrons. The neutron arrival time for the measurements (unlike that for the calculations) is referred to the time between the beam hitting the target and the neutron detected by the detector.

Since the neutron signal is roughly exponential in the arrival time distribution, the inverse of the slope of these curves gives the mean arrival time. Therefore, the estimation of the slope is important for the calculation of the dead time correction factor for moderating type detectors.

1.5 Summary

Thus far, Chapter 1 has given an introduction to the dead time correction and its importance in pulsed radiation fields for moderating type detectors. The objective of the study has also been outlined.

Chapter 2 describes the geometry of the detectors used in this study, namely, the moderated BF_3 detector, AB remmeter, and Bonner Sphere detectors. Section 2.2 provides general discussion of the MCNP code along with some details of the input files developed for this study. In Section 2.3, the tally summary of MCNP output file is discussed. Neutron sources defined for the MCNP calculations are described in Section 2.4.

Chapter 3 describes the neutron arrival time measurements made at FFTB. The location of detectors is described in the Section 3.1. The associated electronics for the timing measurements is described in Section 3.2.

The results of the MCNP calculations are discussed in Section 4.1 of Chapter 4. Section 4.2 gives a comparison between the measurements and the calculations. Section 4.3 is the calculation of the T-values.

Section 5.1 of Chapter 5 is a summary of the study. Conclusions that can be drawn from the study are discussed in Section 5.2. Section 5.3 contains suggestions for further studies.

2. MONTE CARLO CALCULATIONS

2.1 Introduction

The arrival time distributions of neutrons for various detectors are calculated using the latest version of the MCNP4A Monte Carlo Code (MCNP 1993). This chapter describes the basic concept of a Monte Carlo approach and introduces the way the MCNP was used for this study. Geometry of the detectors used in this work is discussed in detail in Section 2.2. Neutron sources (monoenergetic and spectra) used for the calculations are also presented.

The general-purpose Monte Carlo N-Particle (MCNP) code is used for calculating time-dependent continuous-energy transport of neutrons, photons, and/or electrons in three-dimensional geometry. The code provides a number of tally (the desired result) output options and various variance reduction techniques that improve the efficiency of the calculations.

When a neutron travels through a material, it interacts with the constituent atoms of that material. Whether the neutrons become absorbed or scattered depends on the neutron interaction cross section in that material. It cannot be predicted exactly how the particles will interact or how will they travel in the material before being scattered or captured. However, the probability of occurrence of one or the other process can be determined by the relevant cross sections. The cross sections can enable us to predict the distribution of flight distances (mean free path) that a large number of particles would have before the

first interaction. This is done by random-walk analysis in the MCNP code. The random-walk analysis is the statistical history for the life of each particle generated by computer using random numbers.*

The MCNP code has extensive nuclear data and cross section libraries, which enables it to determine which process will occur at a particular time in the life of the particle. The life of a particle begins with its generation from the source and ends when it gets absorbed or scattered to move outside of the detector assembly. The code also takes into account how much energy is lost during each interaction and what is the new direction of the particle (if scattered) or how many neutrons created in any fission event.

A very large number of histories is evaluated to have a good statistics and to approach a more accurate result with a small uncertainty. Records of all the events in the life of the particle and the scored tally/tallies are tabulated in an output file (see Section 2.4).

In this work, the MCNP4A code is used to simulate transport of neutrons from the source to the sensor through different layers of materials, including the moderator. In the sensor, neutron captures are scored as a function of time. The description of the problem is given in an input file (see Section 2.3).

---

*A set of numbers, which have no pattern, that are sampled uniformly between zero and one.

12

2.2 Geometry of detectors

2.2.1 Moderated BF$_3$ detector

A schematic drawing of a custom-made moderated BF$_3$ detector is shown in Fig. 2.1. This detector is specially designed for the neutron fluence measurement. The moderated BF$_3$ detector consists of a BF$_3$ proportional counter (Reuter Stokes RS-P1-1613: 31 cm long and 5 cm in diameter) with an attached preamplifier that is inserted into a cadmium (Cd)-covered polyethylene cylinder. In this device, boron trifluoride (BF$_3$) serves both as a target for conversion of neutron to secondary charged particles as well as a proportional gas. The gas is highly enriched in ^{10}B to increase its efficiency. The absolute pressure in typical BF$_3$ tube is 70 cm Hg. The whole assembly is encased in an aluminum cylinder.

The BF$_3$ gas is a thermal neutron sensor. The thermal neutrons cross section for ^{10}B(n, α)^{7}Li reaction is 3840 barns. Neutrons that have been slowed down to a few hundreds of eV can also react with ^{10}B, however, the reaction cross section varies as $1/v$ and drops to about 100 barns at 100 eV. The reaction may be written as follows :

$$
{}^{10}_{5}B + {}^{1}_{0}n \longrightarrow \left\{
\begin{array}{ll}
 & \\
{}^{7}_{3}Li + {}^{4}_{2}\alpha & \quad Q\text{-}value \\[4pt]
 & 2.792\ MeV\ (ground\ state) \\[4pt]
Li^{\cdot} + {}^{4}_{2}\alpha & 2.310\ MeV\ (excited\ state)
\end{array}
\right.
$$
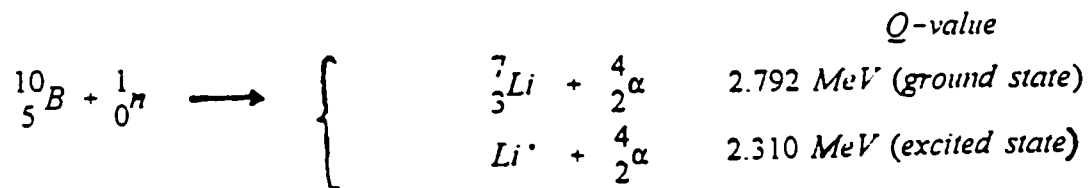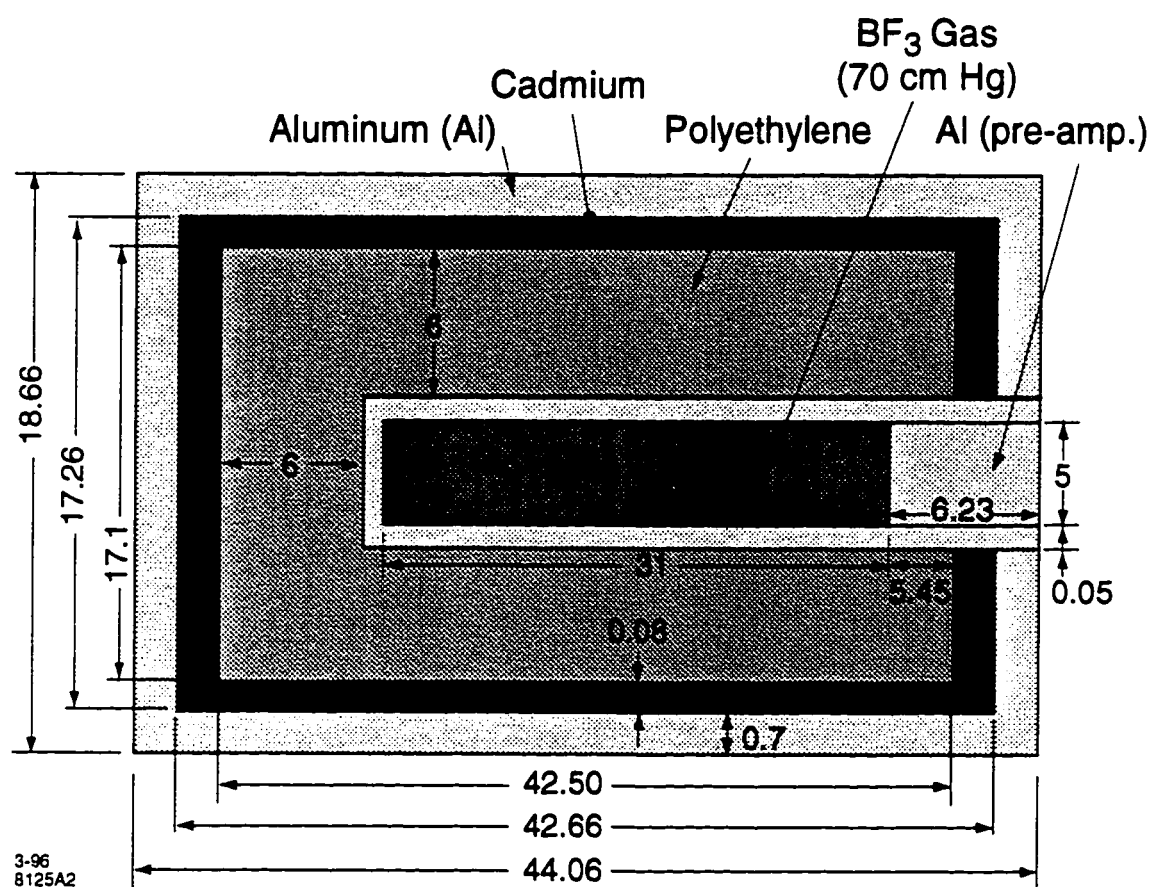
Fig. 2.1 Schematic representation of cross-section of the moderated BF₃ detector.

In either case (ground state or excited state), the Q-value of the reaction is very large compared to the energies of slow neutrons. The energy imparted to reaction products (^{7}Li and α) is the Q-value itself. Any information about the neutron energy is submerged in the much larger reaction energy.

The BF_3 detector is relatively insensitive to gamma rays, because high energy photons lose small fractions of their energy in the detector. The resulting secondary electrons give rise to smaller pulses, whereas the ^{7}Li ion and alpha particles have relatively shorter ranges in the gases and deposit most of their energy (Q-value energy) to give rise to a larger pulse.

As mentioned in Chapter 1, the purpose of the BF_3 detector being inserted in the Cd-covered polyethylene moderator is to use this detector for detecting fast neutrons. Most fast neutrons (above a few MeV) incident on the cylindrical polyethylene moderator (a radial thickness of 6 cm and 42.5 cm long) are slowed down to thermal energy (0.025 eV) before interacting with the BF_3 gas. On the average, the elastic scattering of a fast neutron on hydrogen [in polyethylene $(C_2H_4)_n$] results in the loss of half of the initial neutron energy.

The polyethylene is covered with a 0.08 cm thick layer of cadmium (Cd) to ensure that only epithermal neutrons enter the moderator. Since Cd has a very high thermal neutron capture cross section of 3620 barn, it absorbs essentially all the incident thermal neutrons. Hence, the moderated BF_3 detector responds only to the incident neutrons with energies greater than the Cd cut-off (0.4 eV).

15

2.2.2 Anderson-Braun (AB) remmeter

A schematic drawing of an Anderson-Braun (AB) remmeter is shown in Fig. 2.2a. It has a BF_3 proportional counter as the thermal neutron sensor. The detection technique works the same way as that for the moderated BF_3 detector. The BF_3 tube in this detector is only one third of the size of the one in the moderated BF_3 detector. Since it is designed to measure dose equivalent rate, it is called a remmeter and the structure of its moderator is more complicated. The total thickness of the polyethylene is larger (6.5 + 1.6 = 8.1 cm) than that of the moderated BF_3 detector.

Figure 2.2b shows the (AB) remmeter and its components. A 10.8 cm long and 3.4 cm in diameter aluminum tube is filled with BF_3 gas. The gas has a pressure of 70 cm Hg. The BF_3 tube is surrounded by an inner polyethylene (15 cm long and 1.6 cm radial thickness), covered with a 0.5 cm thick boron plastic cylinder, and an outer polyethylene moderator which is 24.4 cm in length and of 6.5 cm radial thickness.

The boron plastic is boron doped synthetic rubber and has a number of holes in its lateral, front, and end surfaces. The holes are 10 mm in diameter. They cover 22% of the total boron plastic area. The purpose of the boron plastic is to capture some of the thermal and epithermal neutrons. This moderator design simulates an energy response which is close to the fluence to dose equivalent conversion factor curve for fast neutrons (ICRP 1973).

16
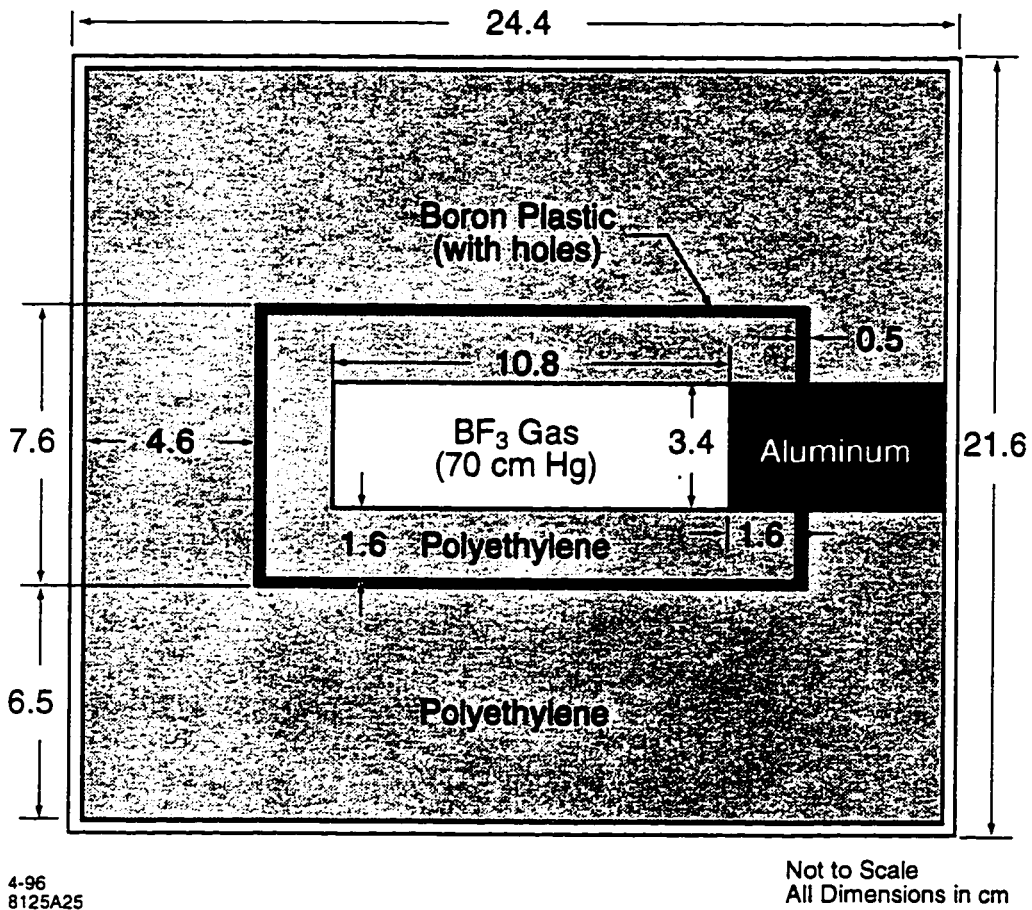
Fig. 2.2a Schematic representation of cross-section of the Anderson-Braun remmeter.
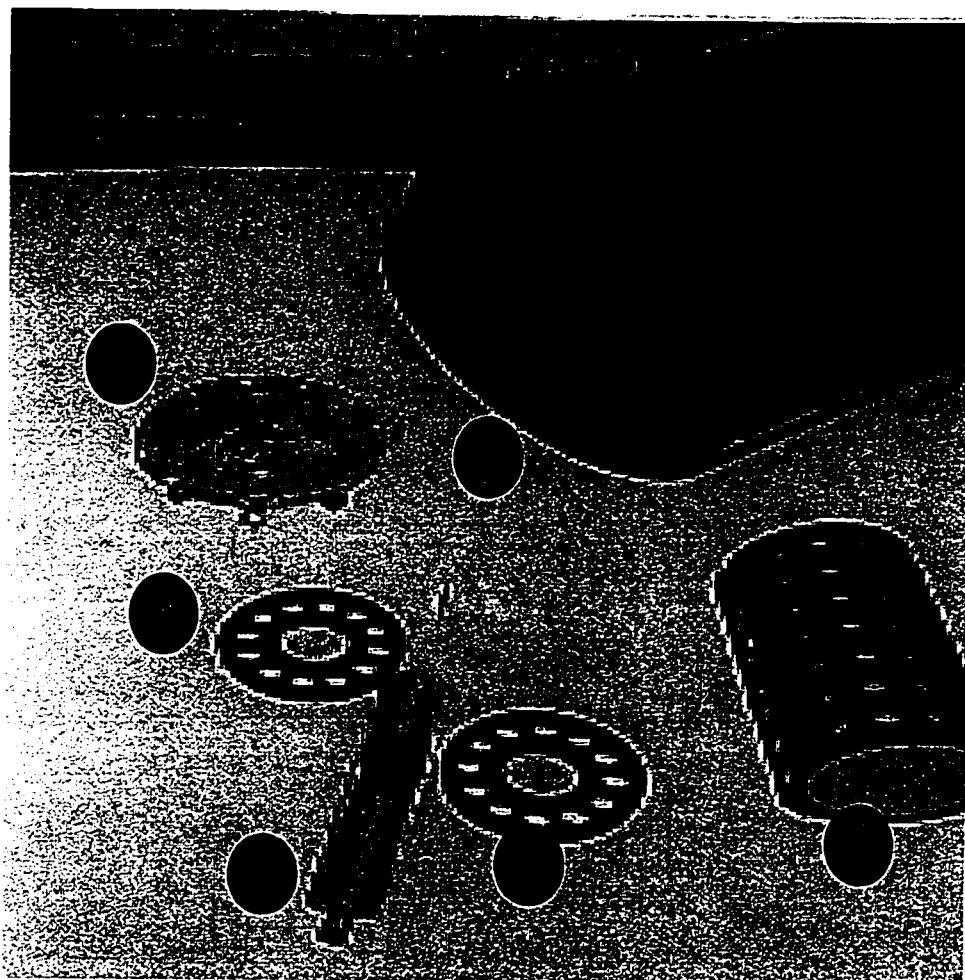
Fig 2.2b The Anderson-Braun (AB) remmeter and its components: 1) The main body of this detector is the large polyethylene cylinder in the background. 2) The Reuter Stokes BF3 tube model RS-P1-0802-104. 3) Smaller polyethylene cylinder with boron enriched plastic cover. 4) Boron enriched plastic end inserts. 5) Aluminum end cap with high voltage connector.

Due to its pseudo-spherical body (24.2 cm x 21.6 cm), the response of an AB remmeter is similar for neutrons incident from the side and that from the end (Liu 1991). During this work, the detector was placed laterally relative to the source direction.

2.2.3 Bonner Sphere detector

A schematic drawing of a Bonner Sphere detector probe is shown in Fig. 2.3a. The detector has a 4 mm x 4 mm enriched ^{6}LiI(Eu) crystal as the thermal neutron sensor. The ^{6}LiI (a scintillator) is coupled to photomultiplier tube (PMT) by a 10 cm long Plexiglas light guide. The scintillator crystal, light guide, and photomultiplier are placed in an aluminum housing; together, they constitute the detector probe. The Bonner Sphere detector probe is placed inside the polyethylene sphere so that crystal lies at the center of the sphere. This is called the detector assembly. Example of placement of sphere over detector probe is shown schematically in Fig. 2.3b.

Neutrons arrive at the center of the moderator as thermal neutrons and interact with the scintillator via ^{6}Li(n, α)^{3}H reaction. The reaction produces a total of 4.79 MeV α and ^{3}H particles that are stopped in the ^{6}LiI(Eu) crystal. The crystal then produces light pulses. The light pulses guided through the light guide reach PMT and are converted to electronic signals that are recorded with the associated counting system.
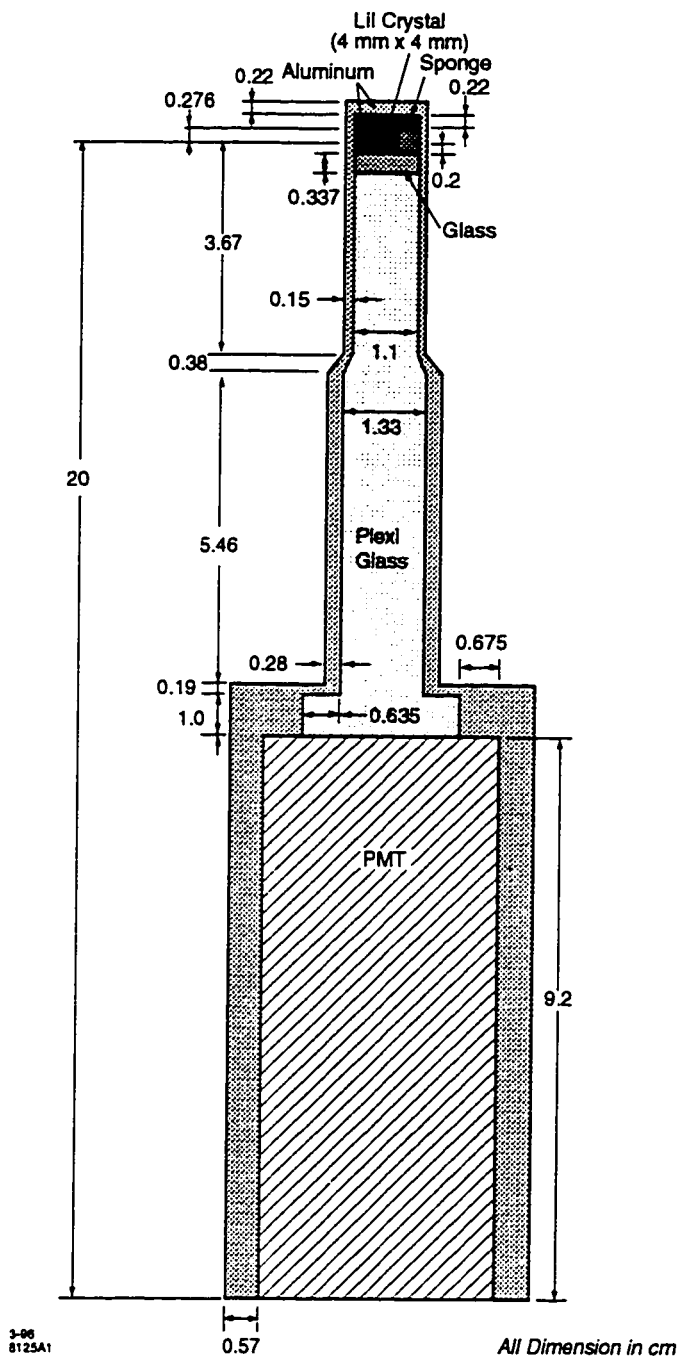
Fig. 2.3a Schematic representation of cross-section of the Bonner Sphere detector probe.

20
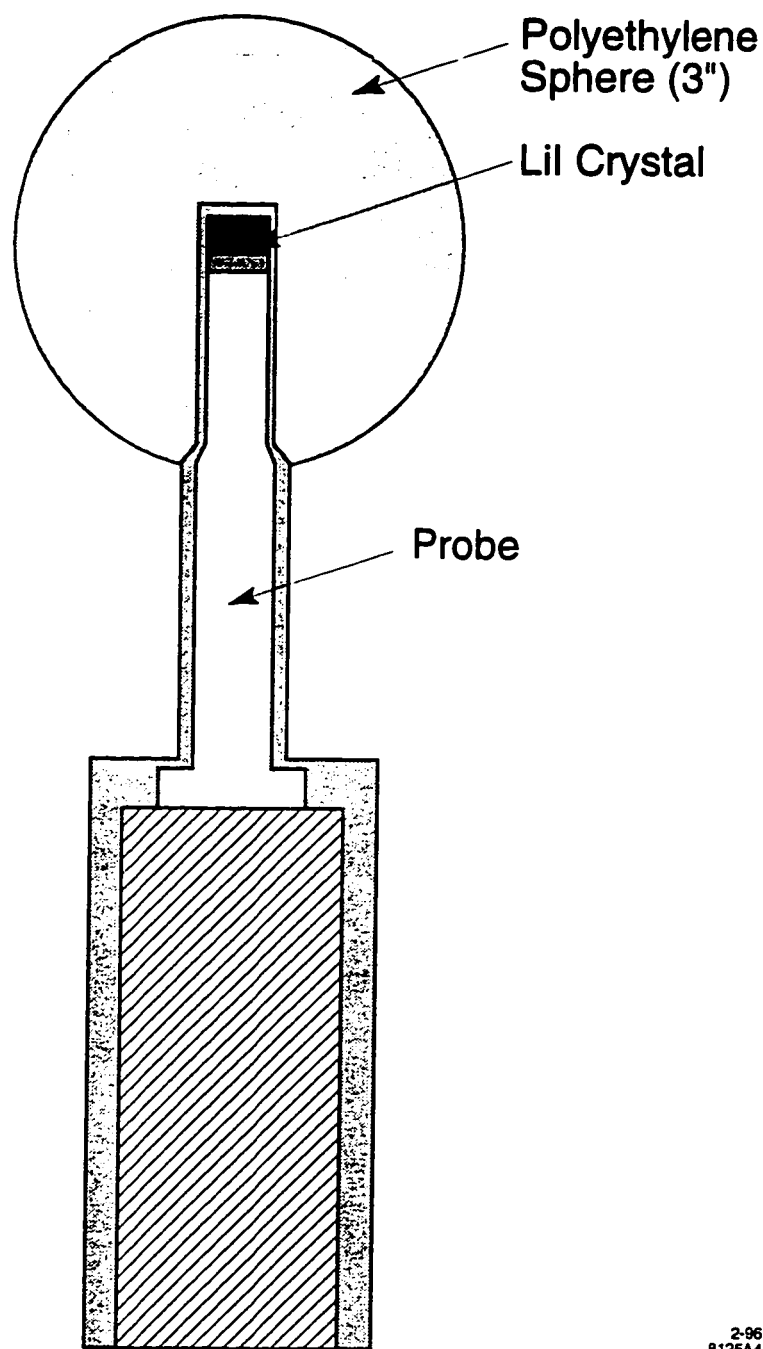
Fig. 2.3b Schematic representation of cross-section of the Bonner Sphere detector assembly.

The response of this instrument as a function of neutron energy varies substantially with the size of the moderator (Knoll 1989). Therefore, polyethylene spheres of various diameters are used to detect neutrons in different energy range. The different thickness of the moderator also affects the neutron arrival time distributions. Being spherical in shape, the angular response of Bonner Spheres detector is almost perfectly isotropic. In this work, the detector was placed in such a position that the probe axis was perpendicular to the incident neutron source.

2.3 MCNP input file

This section briefly describes an MCNP input file. The input file includes the problem geometry, source definition, tallies, material specification, physics of the problem, histories to be run, and the tables desired to be printed in the output file. The MCNP input file consists of these sections: Title card, Cell cards, Surface cards, and Data cards.

Appendix A1 is MCNP input file of the moderated BF_3 detector for monoenergetic neutrons. The geometry of the detector is simulated in details. The BF_3 gas has a density of 0.002567 g/cm^3, with the boron enriched 96% ^{10}B. Density of the polyethylene moderator is 0.95 g/cm^3.

The code models a 20-MeV neutron source incident on the surface perpendicular to the axis of the detector and uniformly distributed over the detector surface. The average neutron flux is scored in the sensor (BF_3 gas) for the reaction (n, α) that is indicated by a

---

* The word "card" is used throughout this chapter to describe a single line output up to 80 characters.

22

reaction number 107. The results are multiplied by a constant 0.024 (atomic density of

BF_3) to include the normalization of "per cm^3" (MCNP 1993). The tally is separated into

50 time bins from 0 μs to 500 μs. Hence, the number of (n, α) reactions per cm^3 in BF_3

are calculated in each time bin.

Appendix A2 is MCNP input file of the moderated BF_3 detector for GRNs. The GRN

spectrum is generated by the MCNP using the relation $P(E) = C\ E\ \exp\ (-E/a)$ for which C

is a constant and the parameter 'a' is set as 1 MeV (MCNP 1993). The MCNP

calculations for FFTB spectrum are done by constructing an input file in which measured

FFTB neutron spectrum is entered as the cumulative source probabilities for various

energy bins (see Appendix A3).

The input files for other detectors were developed in a similar manner by defining

appropriate geometry and material specification. Also, the appropriate tally multiplicative

constant and reaction number are specified for each detector. Appendices B1, B2, and B3

are the MCNP input files of the AB remmeter for monoenergetic 1-MeV neutrons, GRNs,

and the measured FFTB neutron spectrum, respectively. The reaction number for the

remmeter remains the same as 107, because it has the same sensor as that of BF_3 detector.

The tally is separated in 24 time bins from 0 μs to 200 μs. To simplify the geometry input,

instead of defining holes in geometry, a reduced material density is entered on the cell

card. The density of the boron plastic in the remmeter is reduced directly by 22% (from

1.0 to 0.78 g/cm^3).

For the Bonner Sphere calculations, a reaction number 105 is entered which corresponds to $^7Li(n, \alpha)^3H$ reaction in LiI crystal. The multiplicative constant in this case is 0.11733, which is the atom density of LiI. The neutron source is positioned on the plane normal to the probe axis and is uniformly distributed. Appendices C1, C2, and C3 are the examples of the MCNP simulation of monoenergetic 1-MeV neutrons, GRNs, and the measured FFTB neutron spectrum, respectively, for various Bonner Spheres. The polyethylene spheres used for the calculations are of 2″, 3″, 5″, 8″, 10″, and 12″ diameter. The geometry of detector assembly was defined for each sphere in a separate input file.

2.4 MCNP output file

When a problem runs successfully, MCNP loads significant amounts of information in the output file. The tallies are printed in the end portion of the output file as the problem summary. The output file includes the following information:

• Echo of input file.

• Description of cell densities and masses.

• Material and cross section information.

• Neutron creation and loss summary table.

• Problem summary.

• Error analysis table.

A portion of output file of the moderated BF_3 detector for monoenergetic 1-MeV neutrons is shown in Appendix D. It includes the averaged neutron fluence per source

24

neutron for the corresponding time bin with the statistical uncertainties in each time bin. At the end of the tally summary, the total number of scored neutrons in all time bins (1.51896E-05) is also listed. It corresponds to the total area in the arrival time distribution curve. This is the response in counts per incident neutron.

The MCNP code also provides warning messages to inform the user about possible mistakes. The problem, however, will run with the warning messages. All warning messages from an MCNP calculation are examined and understood to be certain that there is no mistake in the problem specification.

2.5 Neutron sources

For the calculation purpose, two types of spectra and various monoenergetic neutrons were defined on the source card of separate input files for each detector. The monoenergetic sources were in the 0.1 eV to 20 MeV energy range.

A GRN spectrum was generated by the MCNP4A code itself by using a value of 1 MeV for the parameter 'a' in the evaporation spectrum formula $P(E) = C\,E\,\exp(-E/a)$. The spectrum is shown in Fig. 2.4. It has a neutron fluence peak at 1 MeV and the intensity drops to minimum at 10 MeV. The spectrum has a small component of low energy neutrons.

The other neutron spectrum was the measured FFTB spectrum (Fig. 2.5) in a 'hot spot' location (Thai 1996), at which the measurements in this work were made. The FFTB spectrum exhibits a two-peak structure.
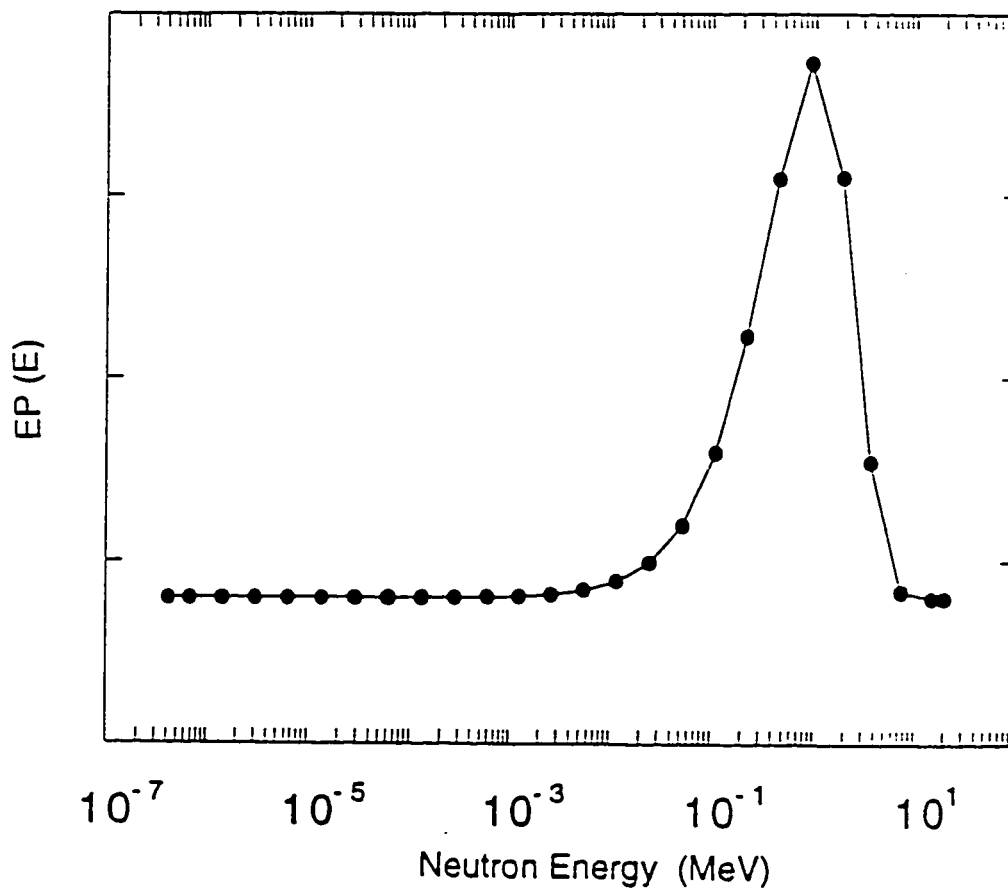
Fig. 2.4 MCNP-calculated GRN spectrum using the parameter 'a' = 1 MeV in the formula P(E) = C E exp (-E/a). Notice that the peak is at 1 MeV.
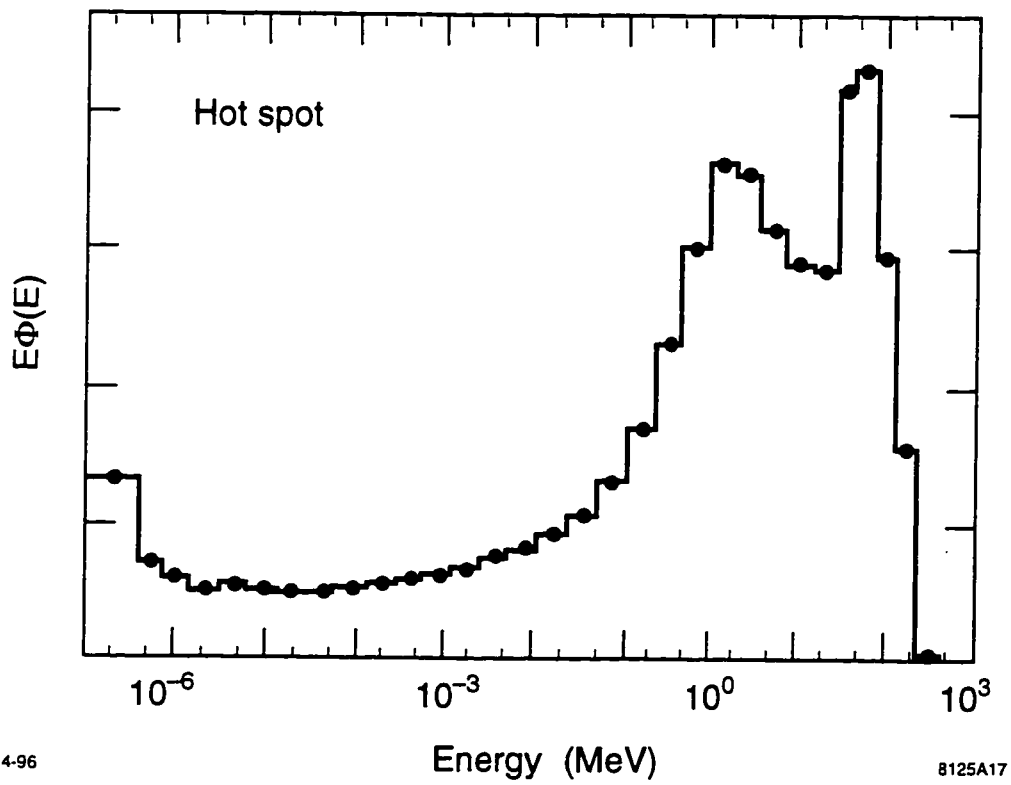
Fig. 2.5 The measured neutron spectrum for FFTB-'hot spot' location. The spectrum has a two peak structure.

The one at higher neutron energy (~100 MeV) results from the slowed-down photopion neutrons. These are the neutrons produced by photopion reaction and have highest energies of all, which could penetrate the thick shielding. The lower energy peak at 1 MeV is generated by the high energy neutrons in the outer layers of shielding.

Both, the GRN and FFTB spectra were simulated up to a 20 MeV neutron energy for the MCNP calculations. This is the upper energy limit in the MCNP code. Therefore, for the measured FFTB spectrum, the neutrons above 20 MeV are not included in the calculations. Due to the low sensitivity of the detector to neutrons above 20 MeV, the calculations without the inclusion of neutrons above 20 MeV are acceptable.

3. MEASUREMENTS

3.1 Introduction

The locations of the various detectors at which the measurements were performed are described in this chapter. The associated electronics and the procedure of collecting data are also discussed.

The measurements for the purpose of our work were possible only when the beam was available for certain high energy physics experimental research. The Final Focus Test Beam (FFTB) facility focuses the 46.7 GeV electron beam to an extremely small size needed for the NLC (Next Linear Collider) project. The beam is then sent to a beam dump which is a metallic cylinder of iron and aluminum. The measurements were performed outside the shielding of the FFTB beam dump on the following days: 12/14/95, 12/19/95 and 12/20/95. During the measurements the electron beam parameters were as follows; beam energy = 46.7 GeV, beam current = 0.7×10^{10} e/pulse, pulse repetition rate = 30 Hz, and the average beam power = 1.56 kW.

The schematic drawing of the location of the detectors outside the FFTB beam dump shielding is shown in Fig. 3.1a. The beam dump is surrounded by 2 to 4 feet of iron and 4 to 5 feet of concrete shielding to reduce the dose rates to acceptable levels. A 22-m-long iron block is placed in the forward direction with respect to the beam to shield against the muons*.

---

* Muons ($\mu^\mp$) are produced in the forward direction, through pair production, the way electrons ($e^\mp$) are.
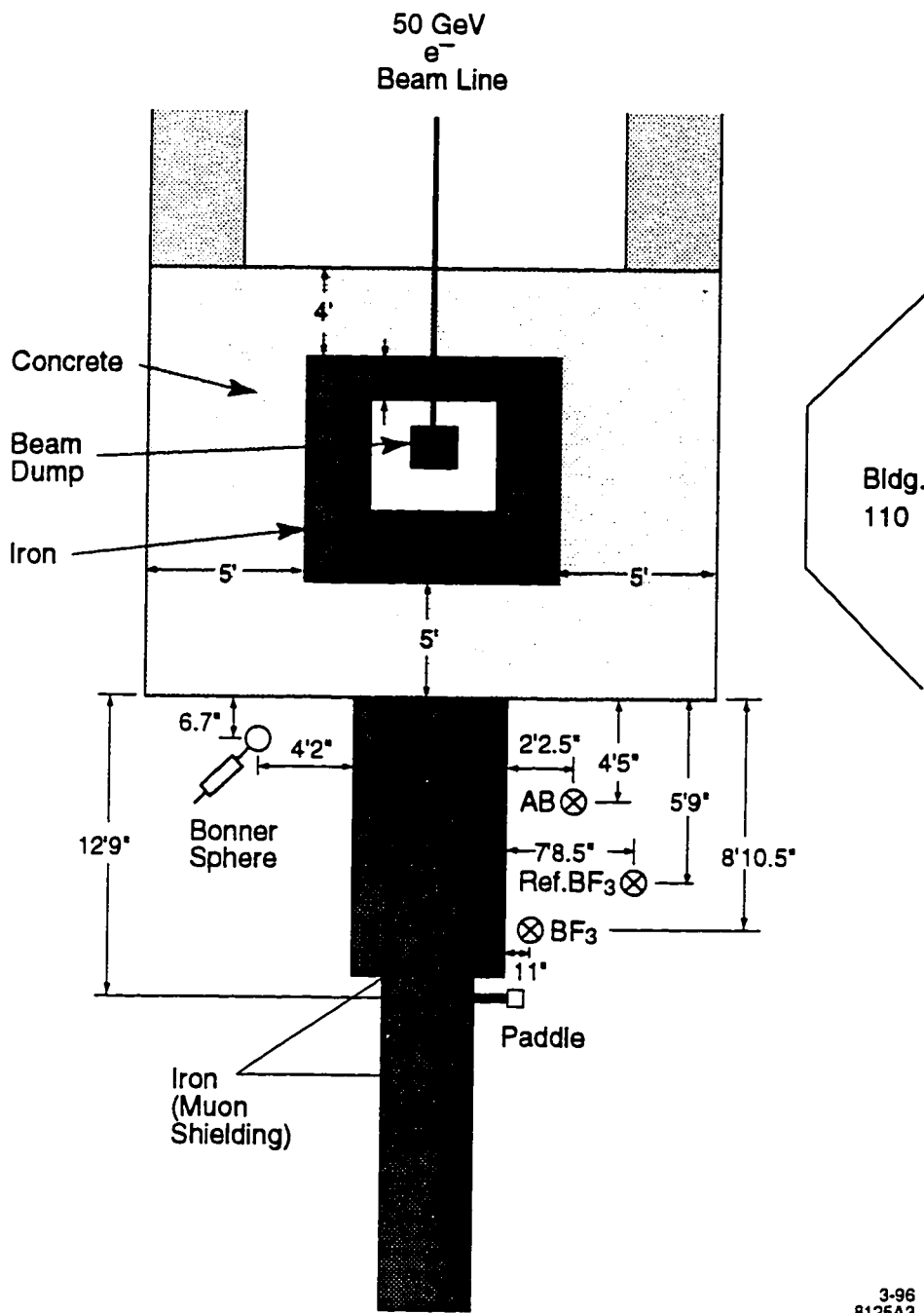
Fig. 3.1a Schematic drawing of the locations of all the detectors for the measurements outside the shielding of FFTB beam dump.

Figure 3.1b shows the placement of two moderated BF_3 detectors, a remmeter and a paddle (the paddle shaped scintillation detector) outside the shielding of the FFTB dump. The paddle was placed on the muon shielding to detect the muons which indicates the presence of the electron beam. The upper right corner of the Fig. 3.1b shows the Bldg. 110 (close to shielding wall) which housed the associated counting electronics. Fig 3.1c shows the location of the Bonner Sphere detector (with 2" polyethylene sphere on the detector probe) on the other side of muon shielding, close to the concrete wall.

All the measurements were made on the ground outside the shielding wall, in the forward direction with respect to the beam. These locations have been found to have the highest dose rates and are called the FFTB 'hot spot' (Thai 1996). The data were collected simultaneously for all detectors at these locations. The data represent the number of neutrons (detected by the sensor of the detector) with respect to their arrival time. The arrival time in the measurements is the period between the instant when the beam hits the target and when the sensor detects the neutrons.

3.2 Electronics

The schematic of the associated electronics for the timing measurements is shown in Fig. 3.2. As shown in this figure, the associated counting electronics for each of the detectors basically consists of a high voltage power supply, an amplifier, and two counters. The Bonner Sphere system has its own high voltage power supply and
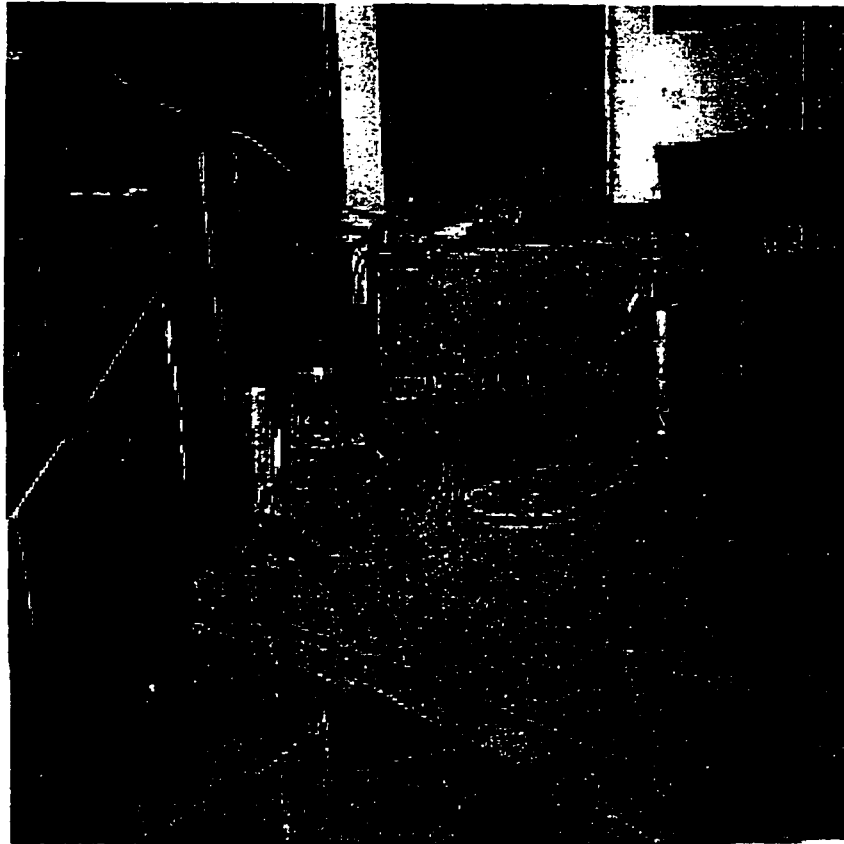
Fig.3.1b The location of the detectors relative to the FFTB concrete shielding (a) and muon shielding (b):
1) a moderated BF_3 detector, 2) a moderated BF_3 reference detector, 3) an AB remmeter, and 4) a paddle detector
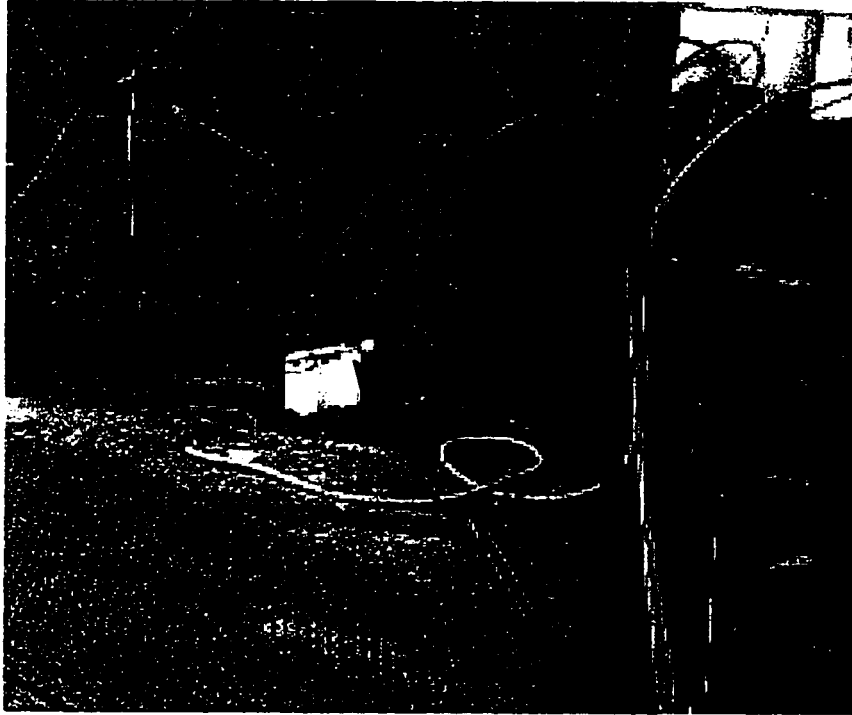
Fig.3.1c The location of the Bonner Sphere detectors (1) relative to the FFTB dump concrete shielding (2) and the iron muon shielding (3)
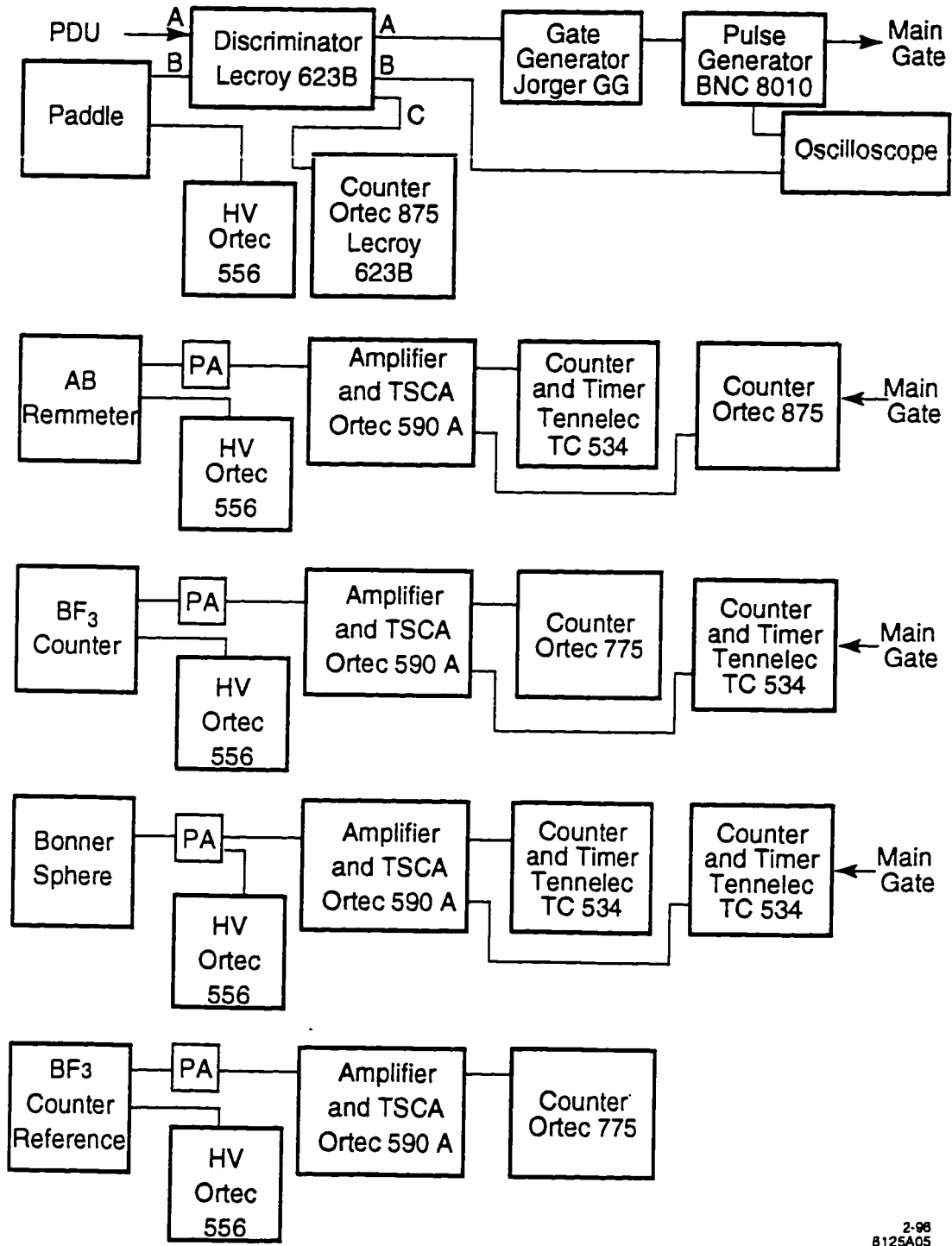
Fig. 3.2 Schematic drawing of the electronics setup for the counting measurements made outside the shielding of FFTB beam dump.

amplifier built in the ORTEC "Nomad" multichannel analyzer as a part of its counting

system. The Bonner Sphere system was operated with the following parameters: high

voltage = +600 V, coarse gain = 100, and fine gain = 2.0. The remmeter was set at high

voltage = +1800 V, coarse gain = 50 and fine gain = 1.5. The settings for two moderated

BF_3 were as follows: high voltage = +1800 V, coarse gain = 50, fine gain =1.5. The

paddle detector was operated with a high voltage supply of -1200 V.

The presence of the beam was detected by the paddle signal. The analog pulse from

the paddle was converted into digital pulse with a discriminator and counted. The leading

edge of this digital pulse indicates the time of occurrence of an input analog pulse (i.e.

electron beam). This signal acts as a trigger to the gate generator and a gate pulse[*] is

generated. Then the gate pulse is used to trigger a pulse generator. The output signal

from the pulse generator constitutes the main gate. The main gate is fed to one of the two

counters of each detector to record the gated signal. The other counter records the

ungated signal.

The combination of the pulse generator and the gate generator enables the gate to be

opened at desired time width. In the absence of the beam, pulses from the PDU[+] (see fig.

3.2) allowed us to set the timing of the gate generating circuit within the resolution of

electronics system. In the presence of the beam, the PDU was adjusted to coincide with

the beam signal.

---

[*] The gate pulse is a standard logic pulse whose width is adjustable.
[+] PDU stands for Programmable Delay Unit and is used to synchronize the timing signal with the beam signal.

35
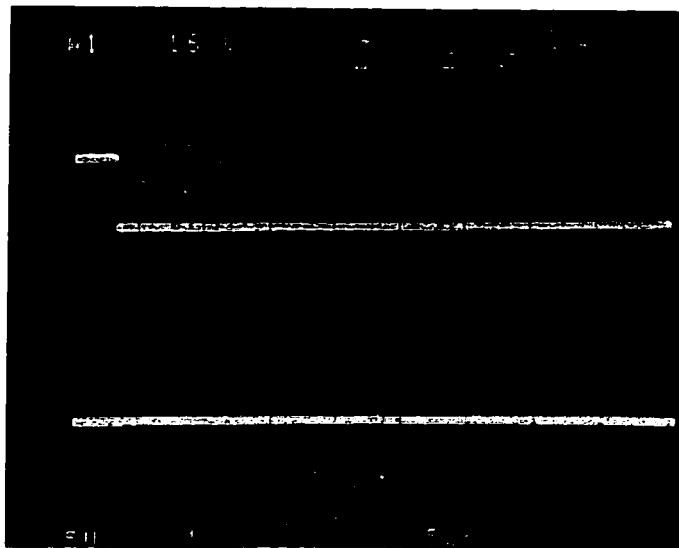
Fig. 3.3a The photograph of the oscilloscope screen displaying that the position of the gate (1) is ahead of the signal from the paddle (2). At this position of the gate, gated counters do not detect any neutrons.

36
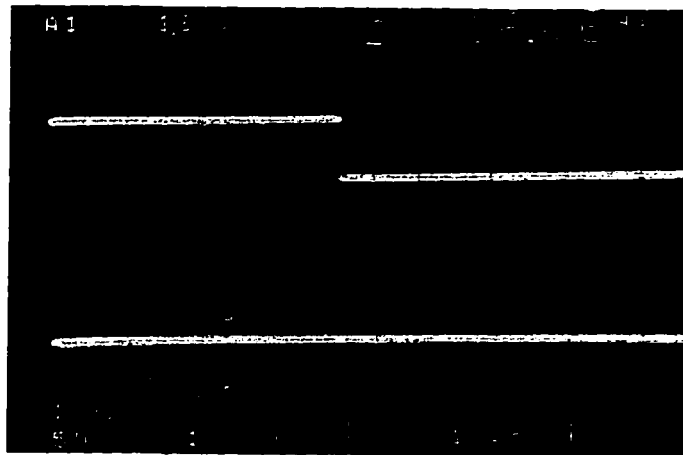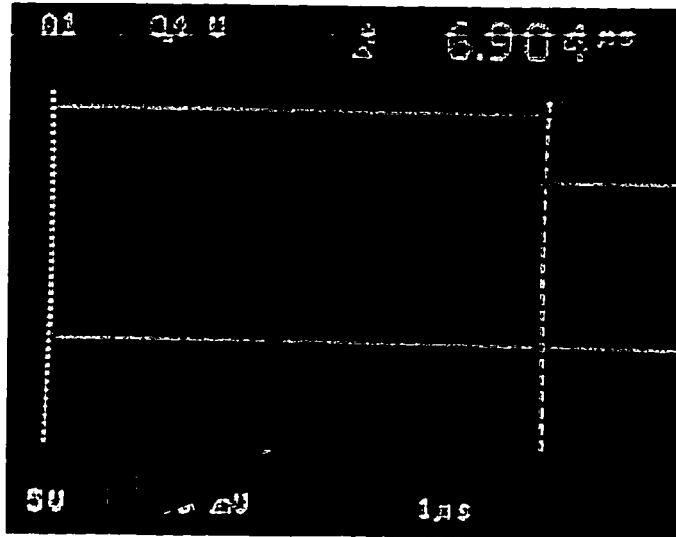
Figs. 3.3b The photograph of the oscilloscope screen displaying the position of the gate (1) and the signal from the paddle (2).

(top) The width of the gate is 6.904 μs and the signal is at 3.8 μs before the gate ends.
(bottom) The gate width is shifted to 40 μs and the signal is at 16.46 μs before the gate ends.

37

Figures 3.3a and 3.3b show the movement of the gate as seen on the oscilloscope screen. In Fig. 3.3a the gate pulse is arriving earlier in time by 23.48 μs than the paddle signal, however, the gate width is only 5μs. At this position of the gate, the detectors do not 'see' any neutrons at gated counters. The width of the gate pulse is then adjusted, so that the gate is open when neutrons arrive. Figure 3.3b show the different widths of the gate relative to the beam signal.

The gate width was increased in appropriate steps starting from the 2 μs time bin. In each time bin, the gated signal was recorded for every detector except for the reference moderated BF_3 detector. The ungated signal was also recorded for all the detectors in the same setup.

The gated signal in each time bin represents the cumulative number of neutrons detected by the sensor within that time. The ungated signal refers to the total number of the neutrons detected by the sensor over all time bins. The gated and ungated signal for each detector were normalized to the reference moderated BF_3 detector signal. These data were used to generate neutron arrival time distribution, which is a differential plot of the number of the neutrons as a function of their arrival time. The uncertainty in the differential representation of the data was large, and therefore, the integral representation of the data (ratio of gated to ungated signal) was used for the analysis.

The timing measurements for the moderated BF_3 detector were also made previously (Rokni 1996) and had better statistics than the present work. The data taken previously were used for the analysis in this work.

4. RESULTS AND DISCUSSION

4.1 Calculations

4.1.1 Moderated BF$_3$ detector results

The results of the MCNP calculations for the moderated BF$_3$ detector are given in

Figs. 4.1a, b, c, and d. The curves shown in these figures are called the neutron arrival

time distributions. Figs. 4.1a, b, and c are the MCNP simulations for monoenergetic

neutrons incident on the surface of the detector. Figure 4.1d shows the comparison of the

arrival time distributions of 1 MeV neutrons with those of GRN and FFTB spectrum.

The data used to generate these plots were obtained directly from the respective

MCNP output files, example of which is shown in Appendix D. This portion of output file

includes the number of neutron reactions in the sensor per source neutron and their

uncertainties in the corresponding time bins. The total number of reactions across all time

bins is also listed, which corresponds to the total area of the curve. For example, in the

moderated BF$_3$ detector, 1 MeV neutrons have 1.51896 E-05 reactions per incident

neutron in total (with a fractional uncertainty of 0.0042). The incident surface area of the

detector multiplied by this number gives the response of detector. The response of a

detector is defined as counts per unit fluence [cm^2]. The calculated response function of

the moderated BF$_3$ detectors for incident from the side is given in Fig. 4.1e. It shows that

the detector is most sensitive to 1 MeV neutrons. The statistical uncertainties in the

calculations of all the neutron arrival time distributions for moderated BF$_3$ detector are
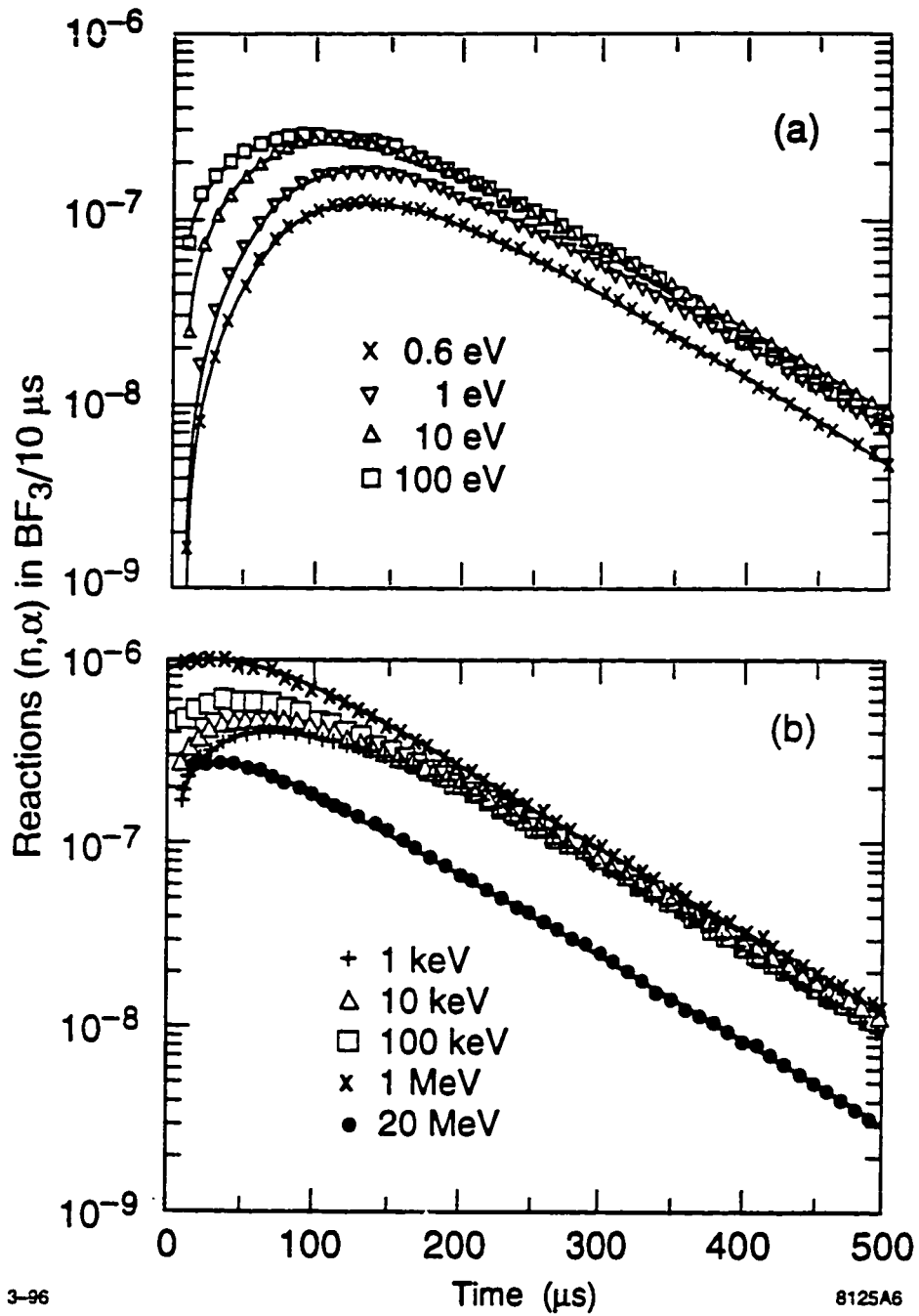
Figs. 4.1 a and b MCNP-calculated neutron arrival time distribution in the moderated BF₃ detector for monoenergetic neutrons. (a) for 0.6 eV - 100 eV (b) for 1 keV - 20 MeV.
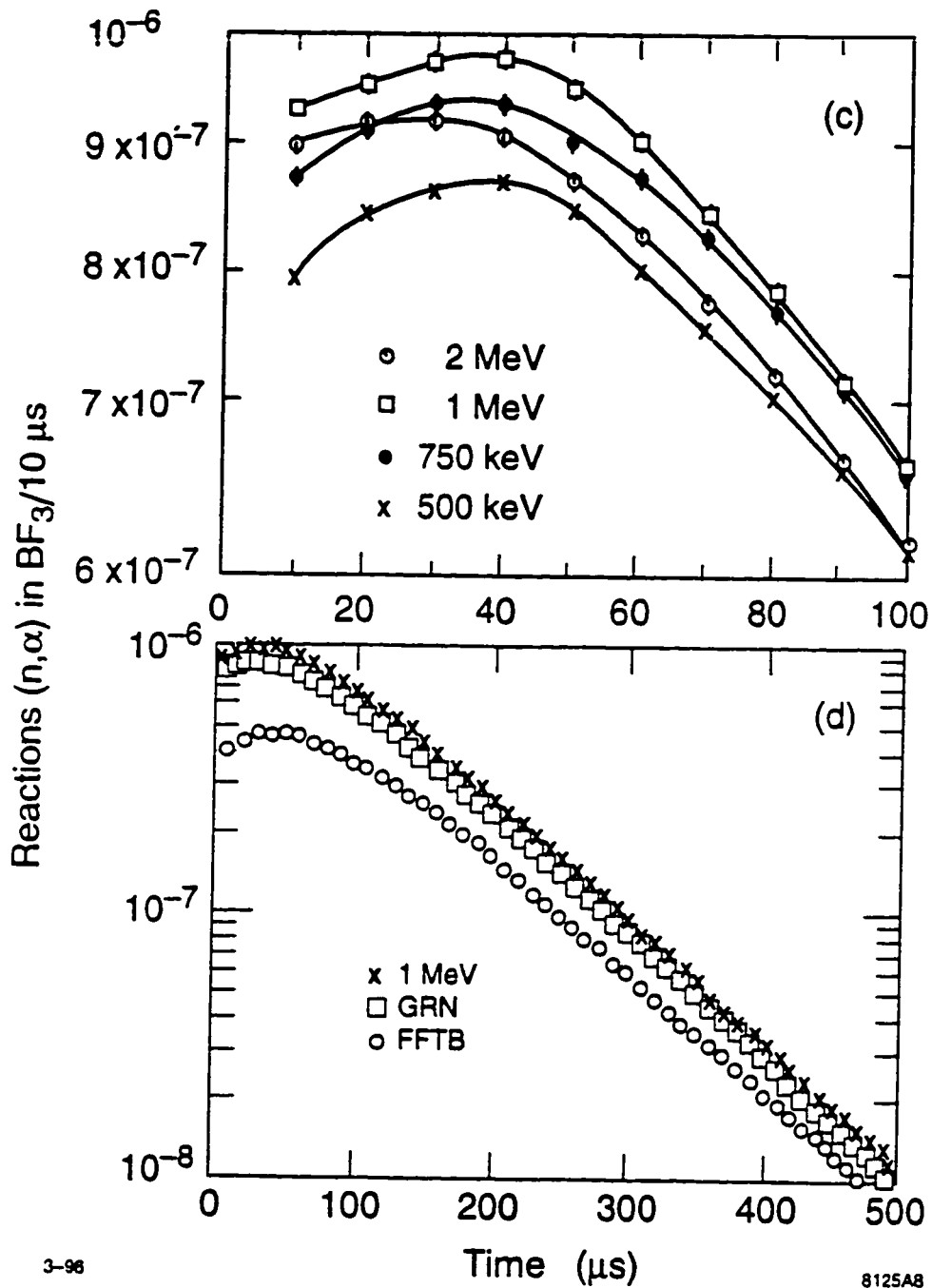
Figs. 4.1 c and d. MCNP-calculated neutron arrival time distribution in the moderated BF₃ detector (c) 500 keV - 2 MeV (d) for GRN and FFTB measured neutron spectrum.

41
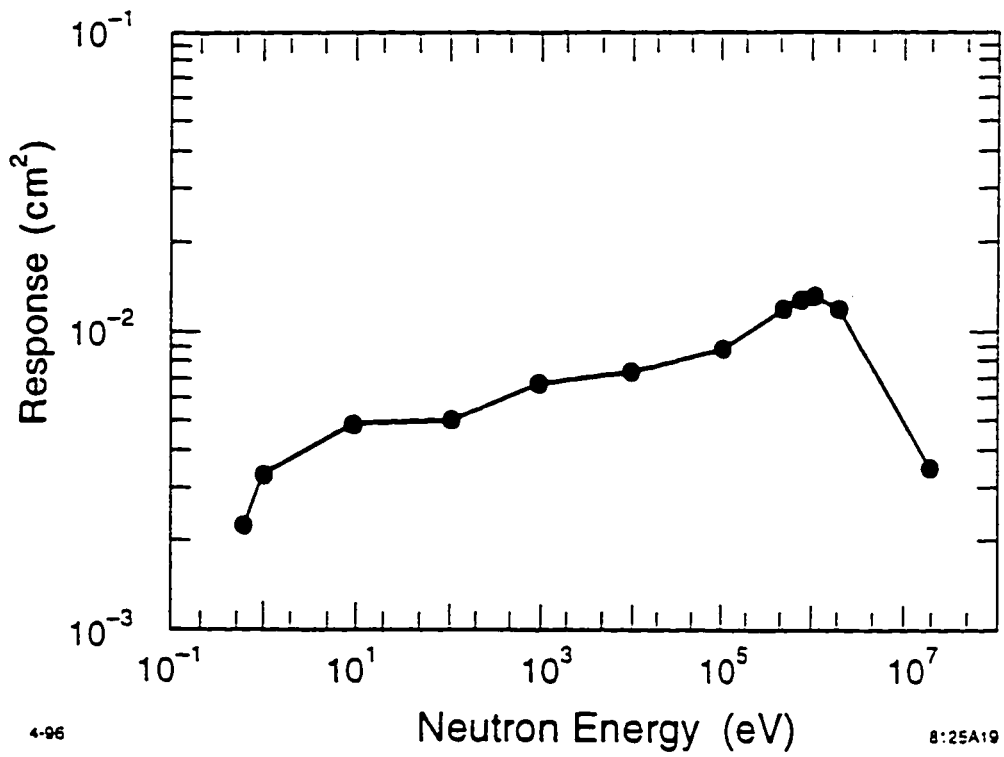
Fig. 4.1e. MCNP-calculated response of the moderated BF₃ detector for the neutrons incident from the side.

42

less than 4% for most cases. Note that there is a noticeable peak shift in various neutron arrival time distributions for different neutron energies. It is clear from Figs. 4.1 a, b and c that the high energy neutrons are reaching the sensor faster than the lower energy neutrons. For example, 1 eV neutrons have a peak at approximately 140 μs (Fig. 4.1 a), whereas 1 MeV neutrons have a peak at about 40 μs (Fig. 4.1 c). The shift in the peak may be explained qualitatively as follows.

When high energy neutrons (e.g., 1 MeV) enter the detector, they penetrate deep into the polyethylene moderator as nearly uncollided fast neutrons, because of the low interaction cross section (larger mean free path). Therefore, the slowing down interactions of the fast neutrons may occur relatively near the sensor. The resulting slow neutrons have to diffuse through a short distance to reach the sensor and be detected.

On the other hand, the low energy neutron (e.g. 1 eV) do not travel deep into polyethylene before their first interaction because of their smaller mean free path. They lose most of the initial kinetic energy and become thermalized near the surface. These slowed-down neutrons have to diffuse through a thicker moderator layer to reach the sensor, compared to the case of incident fast neutrons. Therefore, low energy incident neutrons will be detected later in time than the high energy neutrons.

The total area in Fig.4.1d shows that the moderated BF_3 detector has higher response to 1 MeV neutrons than the GRN or FFTB spectra. This is due to the fact that GRN and FFTB spectra include a number of neutrons above and below 1 MeV neutrons respectively, to which the detector is less sensitive. The neutron arrival time distributions

43

for GRN and measured FFTB spectra are very close to that of 1 MeV neutrons, and both spectra have peak at 1 MeV. Figure 4.1e shows that the MCNP-calculated response of moderated BF_3 detector has a peak at 1 MeV. The response calculations are in close agreement with those done in the past for a similar moderated BF_3 detector having a 6 cm radial thickness of polyethylene moderator (Kosako 1985).

4.1.2 Anderson-Braun remmeter results

Figures 4.2 a and b show the results of MCNP simulation of monoenergetic neutrons incident on the AB remmeter. Fig. 4.2c shows a comparison of results of the GRN and FFTB spectrum with that of 1 MeV monoenergetic neutrons. The data for these plots were obtained in a similar way as that used for the moderated BF_3 detector. Calculated response of the AB remmeter is shown in Fig. 4.2d, which has a peak at about 2 MeV. The data used to generate response curves of the AB remmeter, as well as that of moderated BF_3 detector are given in Appendix E. The statistical uncertainties in the AB remmeter calculations are very small (< 3 %), except for the 10 eV neutrons for which the error is about 18%.

The shift in the peak of the arrival time distribution as a function of neutron energy is also observed here. The remmeter also has a lower response for the FFTB spectrum than for GRN and 1-MeV neutrons.

44
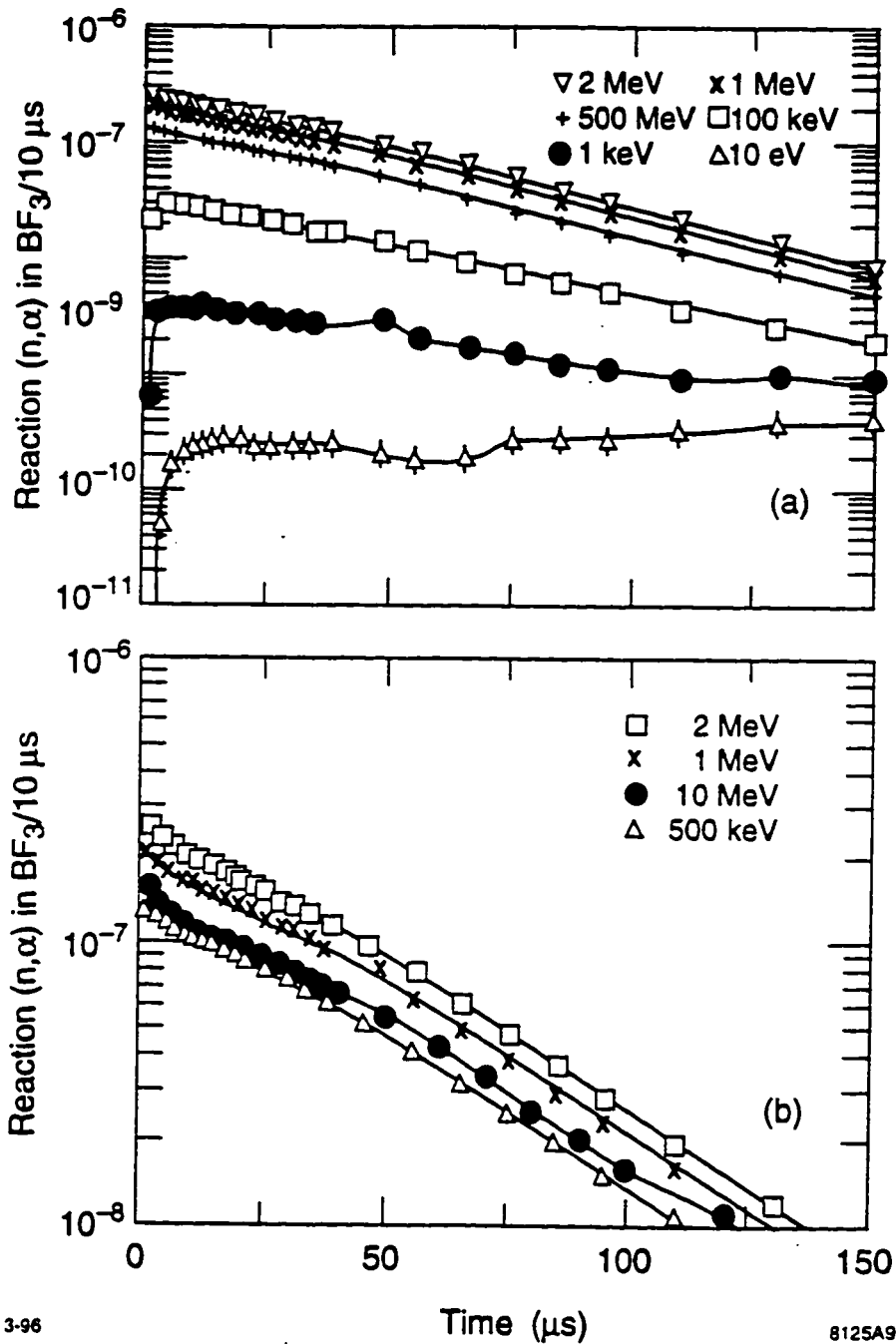
Figs. 4.2a and b. MCNP-calculated neutron arrival time distribution in the Anderson-Braun remmeter for monoenergetic neutrons.(a) for 10 eV - 2 MeV (b) for 500 keV - 10 MeV.
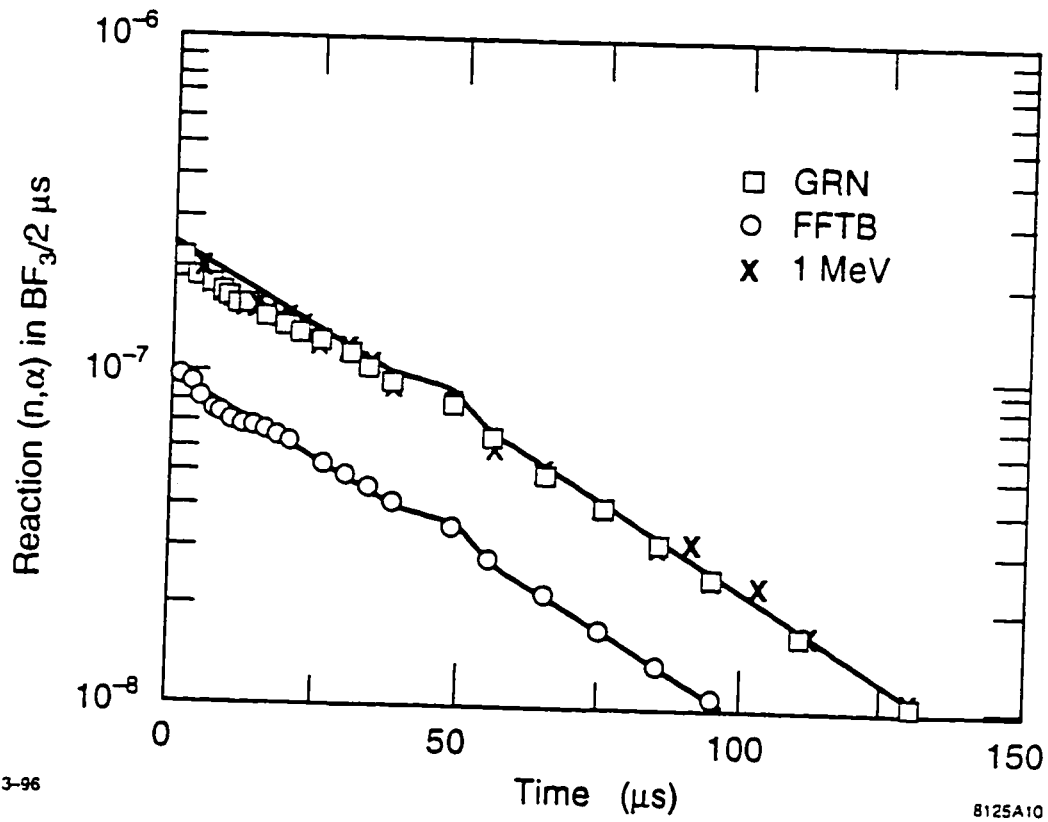
Fig. 4.2c. MCNP-calculated neutron arrival time distribution in the <u>Anderson-Braun</u> <u>remmeter</u> for GRN and FFTB measure neutron spectrum compared with that for 1 MeV neutrons.
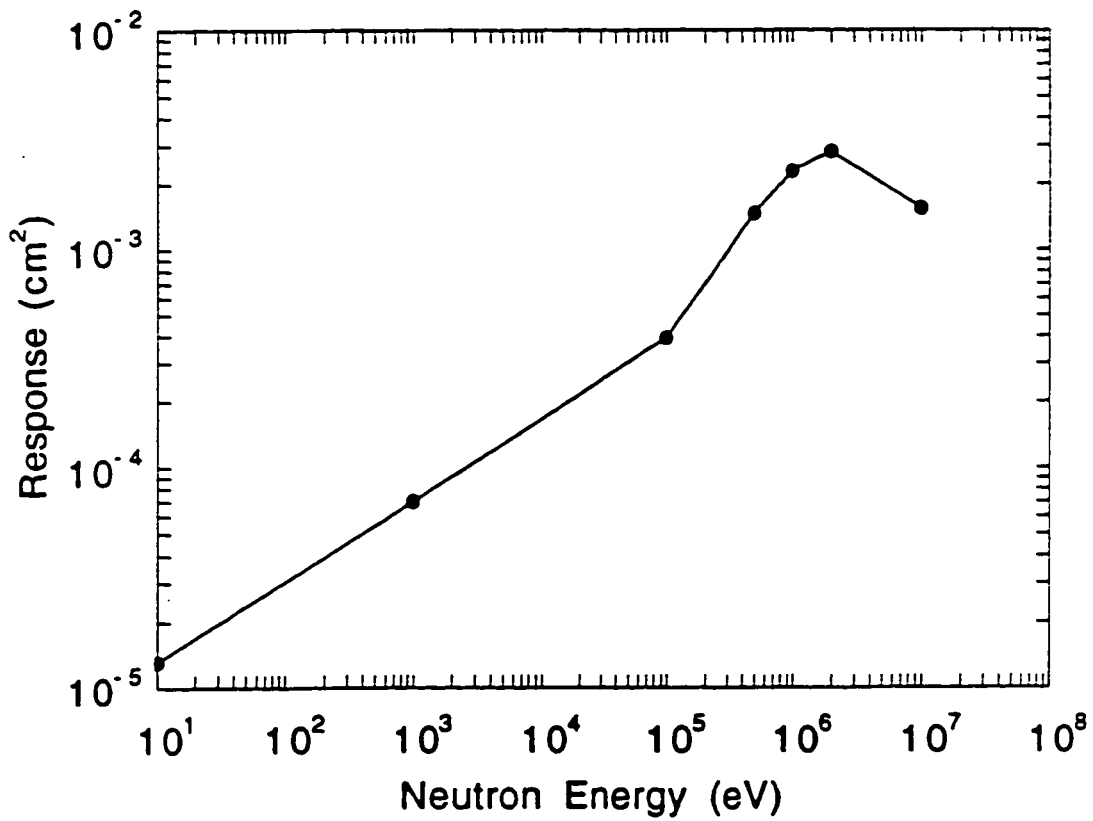
Fig. 4.2d. MCNP-calculated response of the Anderson-Braun remmeter. Note that the counts are per unit fluence.

4.1.3 Bonner Sphere results

The results of the MCNP calculations for some monoenergetic, GRN and FFTB

neutrons are given in Figs. 4.3 through 4.8 for the Bonner Sphere detectors with

polyethylene spheres of 2″, 3″, 5″, 8″, 10″, and 12″ diameter, respectively.

The neutron arrival time distributions for all the Bonner Spheres have a spike at the

beginning of the curve. It might be explained by the fact that the cross section for ^{6}Li

$(n,\alpha)^3$H reaction has a pronounced resonance peak at a neutron energy of about 250 keV.

Therefore, the incident fast neutrons component around the resonant region entering the

LiI crystal is detected with a higher efficiency. However, the 1 keV curve also exhibit a

spike, so the above explanation does not fully account for this effect. It should be noted

that neutron arrival time distribution curves of 8″, 10″, and 12″ Bonner Sphere for GRNs

have been smoothed.

The responses of these detectors are tabulated in Tables 1, 2, and 3. The calculated

response functions for all spheres are reasonable and have the expected shape. The

smaller Bonner Spheres (2″, 3″, and 5″) have high response at low energies (few eV to

keV) whereas the response peak shifts to higher energies (100 keV to few MeV) for larger

spheres (8″, 10″, and 12″).

For the Bonner Sphere detector with a larger moderator, the arrival of low energy

neutrons is delayed by a significant amount of time. For example 0.1 eV neutrons in 10″

Bonner Sphere detector arrive at the sensor after 140 μs (Fig. 4.7a) and for 12″ Bonner

Sphere, even 100 eV neutrons do not reach the detector until 140 μs (Fig. 4.8a).
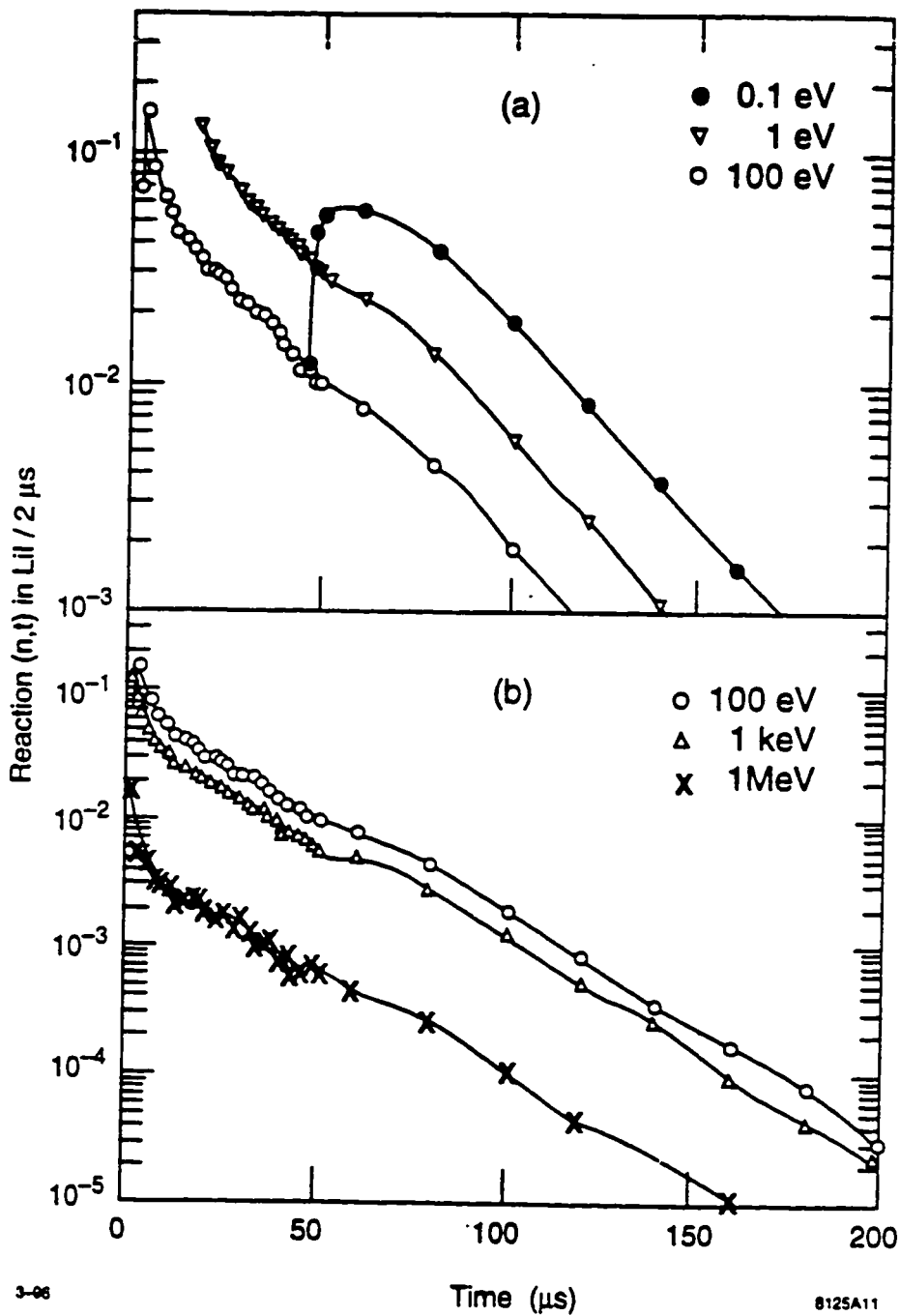
Figs. 4.3a and b. MCNP-calculated neutron arrival time distribution in the 2″ Bonner Sphere detector for monoenergetic neutrons.
(a) for 0.1 eV - 100 eV (b) for 100 eV - 1 MeV.
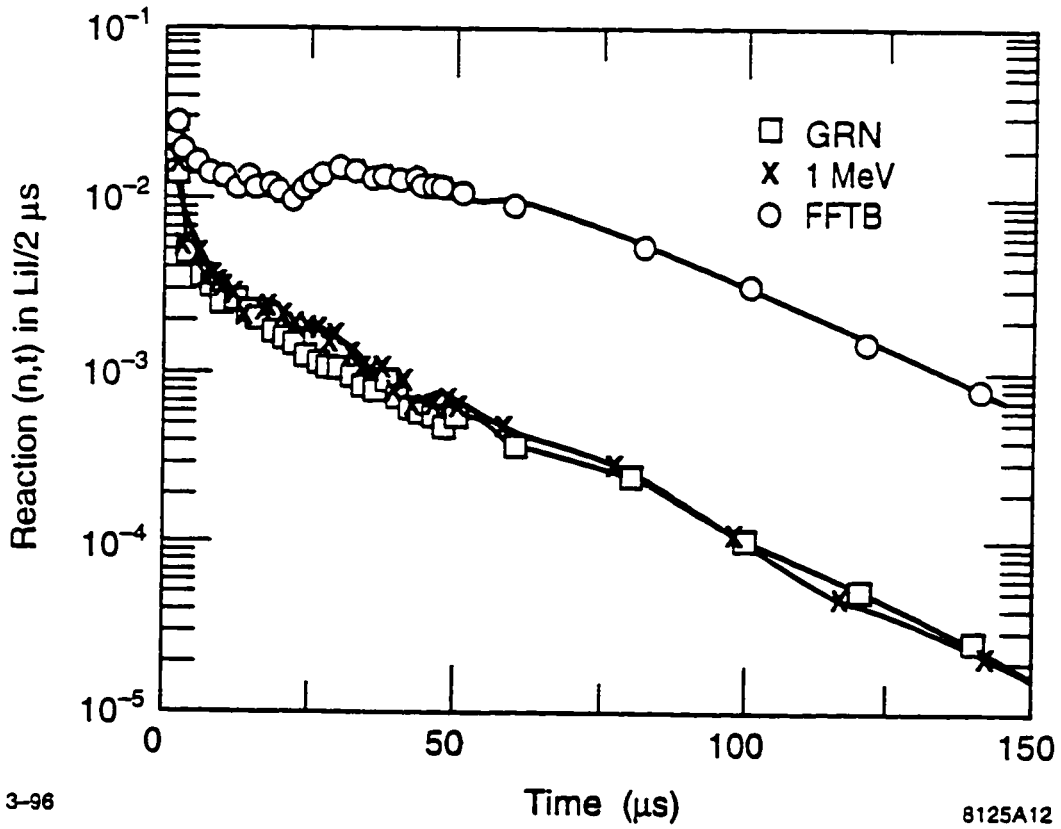
Fig. 4.3c. MCNP-calculated neutron arrival time distribution in the 2″ Bonner Sphere detector for GRN and FFTB measured neutron spectrum compared with that for 1 MeV neutrons.

50
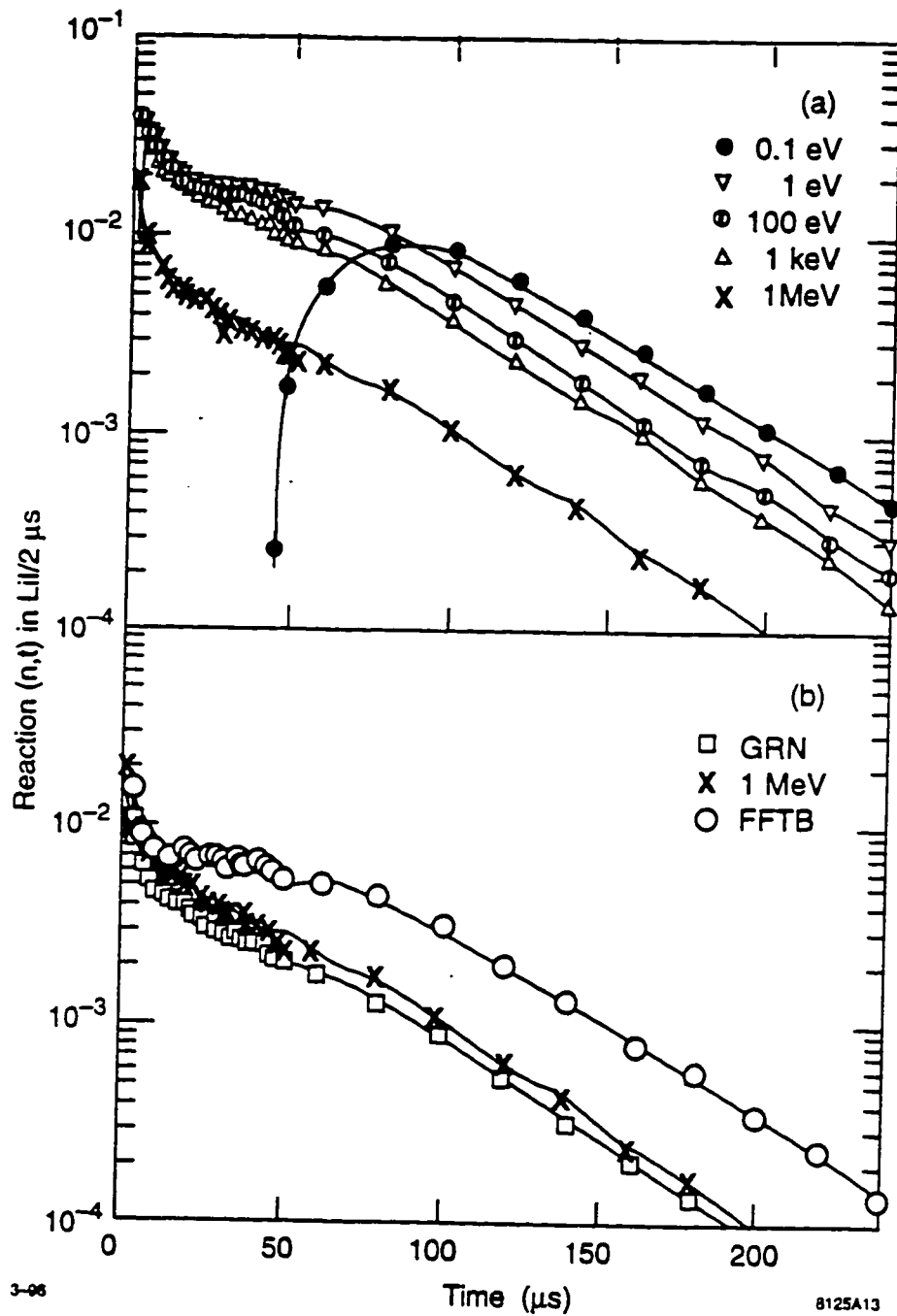
Figs. 4.4a and b. MCNP-calculated neutron arrival time distribution in the 3″ Bonner Sphere detector (a) for monoenergetic neutrons (b) for GRN and FFTB measured neutron spectrum compared with that for 1 MeV neutrons.
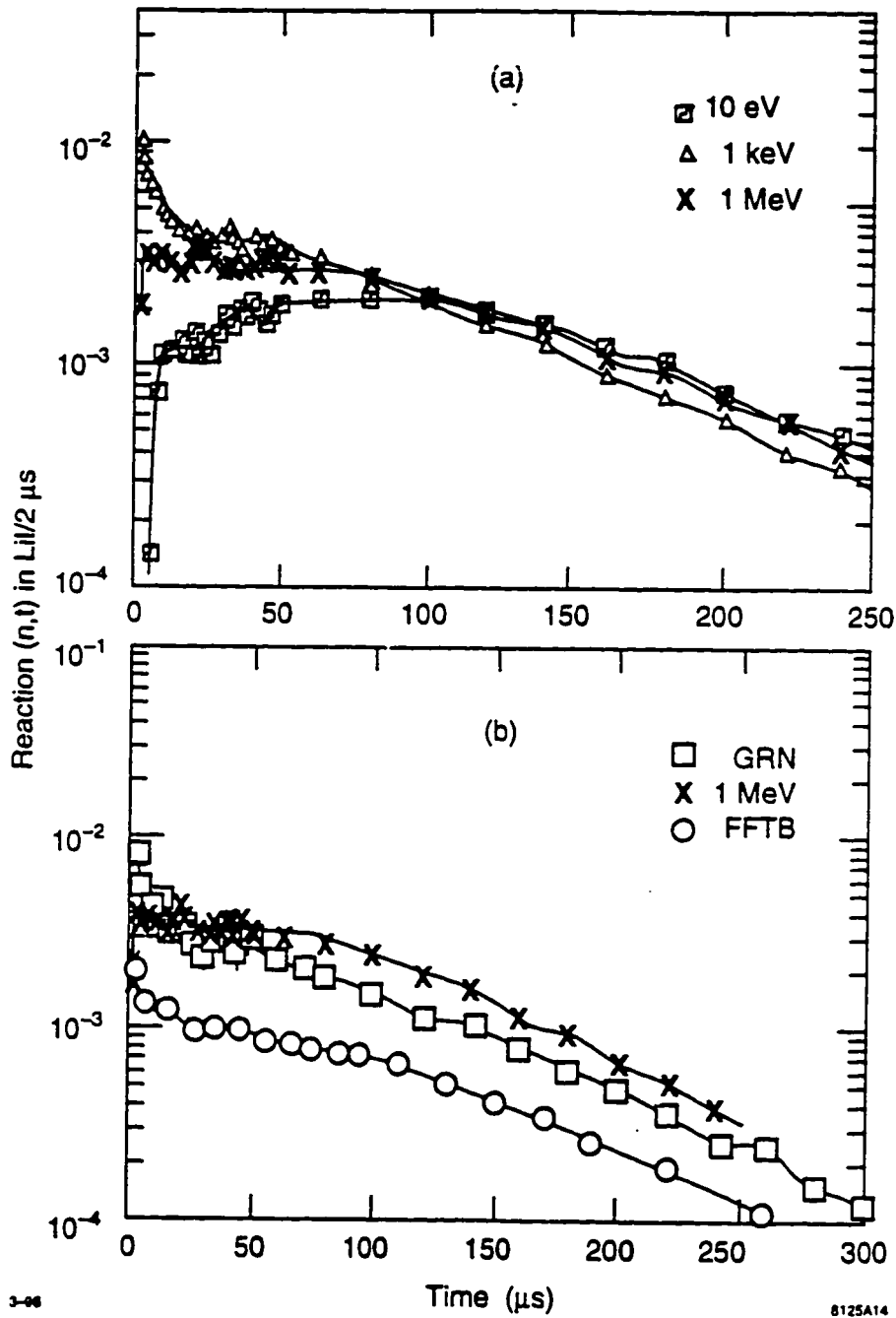
Figs. 4.5a and b MCNP-calculated neutron arrival time distribution in the 5" Bonner Sphere detector (a) for monoenergetic neutrons (b) for GRN and FFTB measured neutron spectrum compared with that for 1 MeV neutrons.
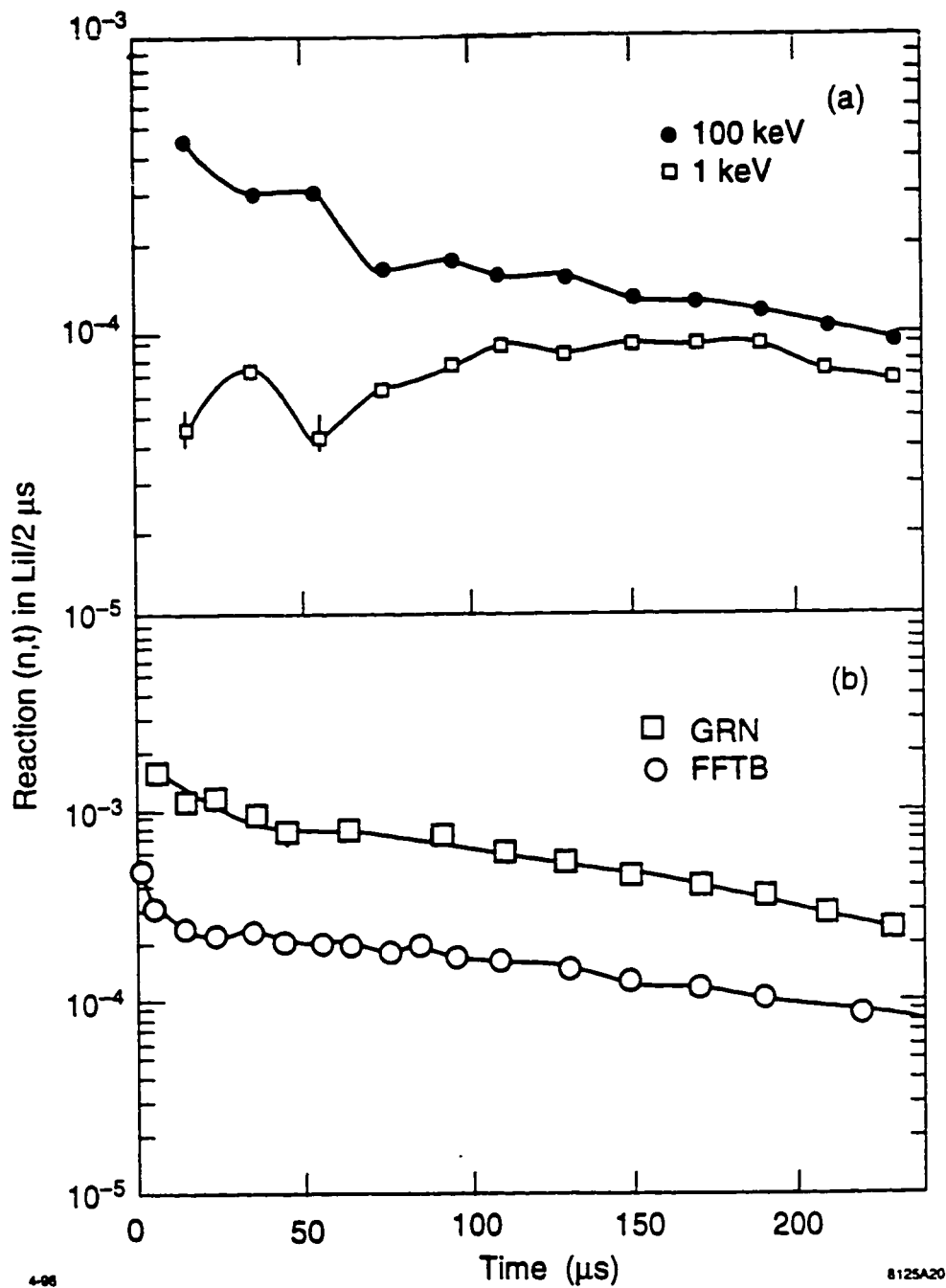
Figs. 4.6a and b MCNP-calculated neutron arrival time distribution in the 8″ Bonner Sphere detector (a) for monoenergetic neutrons (b) for GRN and FFTB measured neutron spectrum.
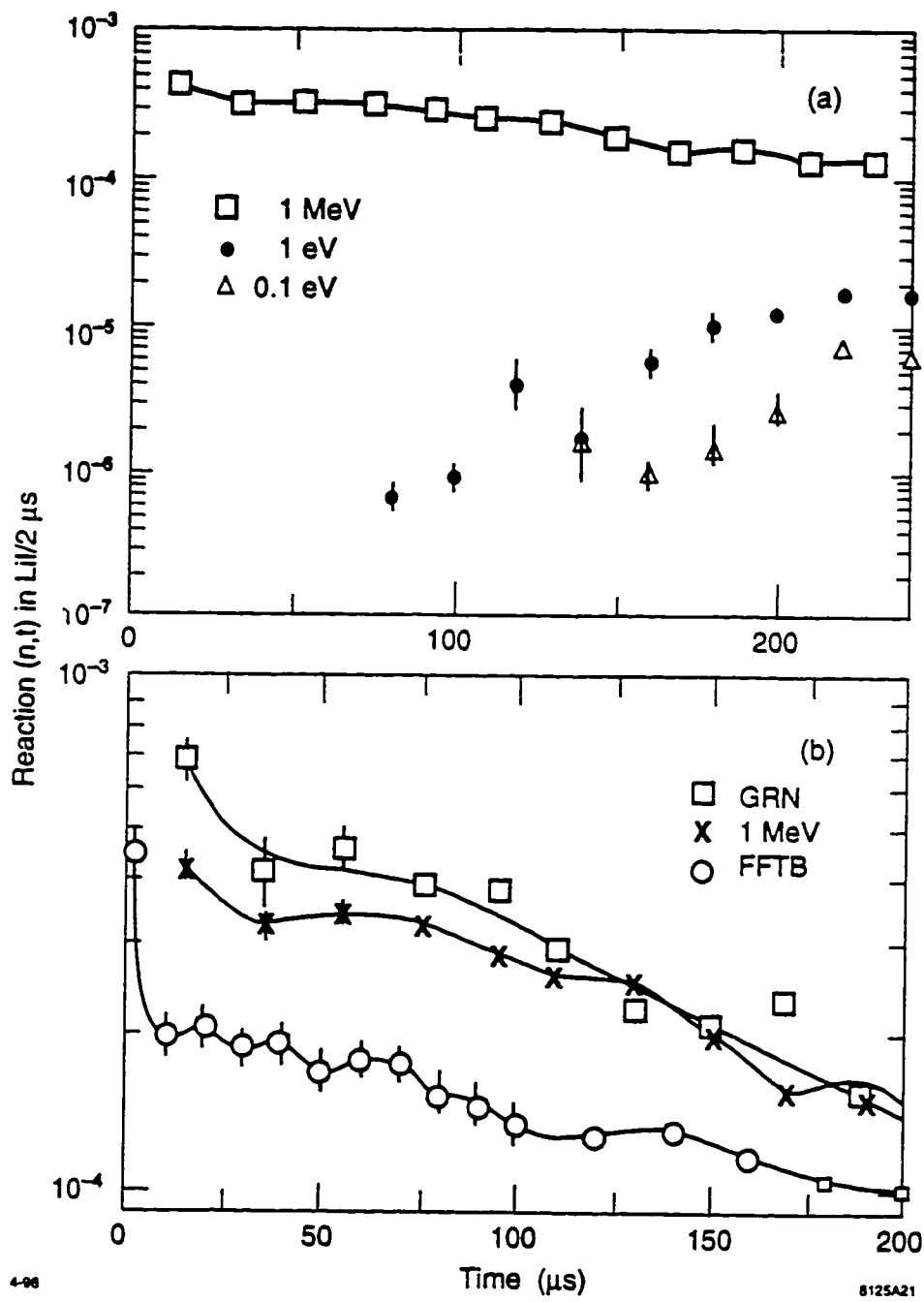
Figs. 4.7a and b MCNP-calculated neutron arrival time distribution in the 10" Bonner Sphere detector (a) for monoenergetic neutrons.(b) for GRN and FFTB measured neutron spectrum compared with that for 1 MeV neutrons.
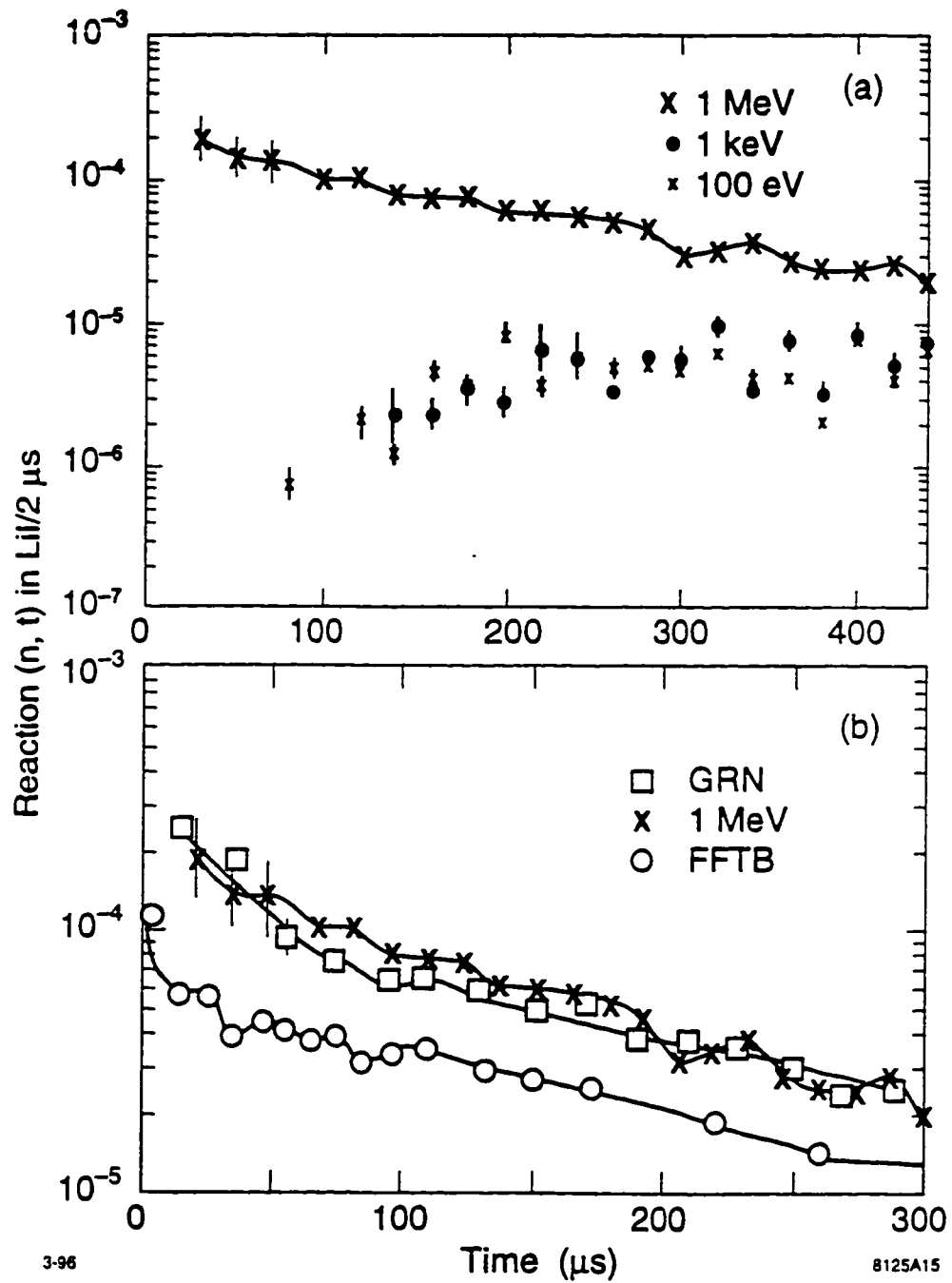
Figs. 4.8a and b MCNP-calculated neutron arrival time distribution in the 12″ Bonner Sphere detector (a) for monoenergetic neutrons (b) for GRN and FFTB measured neutron spectrum compared with that for 1 MeV neutrons.

Table 1. MCNP Calculations of response of 2″ and 3″ Bonner Sphere detector.

Energy	2″ Bonner Sphere (20.30 cm²)[a]			3″ Bonner Sphere (45.60 cm²)[a]		
	Counts [b]	Error (%)	Response [c] [cm²]	Counts [b]	Error (%)	Response [c] [cm²]
0.1 eV	1.09	0.43	22.03	0.38	0.66	17.12
0.6 eV	—	—	—	—	—	—
1 eV	1.52	0.35	30.82	0.66	0.51	30.15
10 eV	—	—	—	—	—	—
100 eV	1.00	0.56	20.34	0.72	0.49	32.72
1 keV	0.68	0.50	13.84	0.61	0.53	27.90
10 keV	—	—	—	—	—	—
100 keV	—	—	—	—	—	—
500 keV	—	—	—	—	—	—
750 keV	—	—	—	—	—	—
1 MeV	0.07	1.54	1.38	0.19	0.96	8.47
2 MeV	—	—	—	—	—	—
10 MeV	—	—	—	—	—	—
20 MeV	—	—	—	—	—	—
GRN	0.06	1.62	1.15	0.15	0.62	6.65
FFTB	0.49	0.22	10.00	0.33	0.71	15.22

[a] cross sectional area of the detector

[b] number of reactions per source neutron in LiI

[c] per unit fluence

Table 2. MCNP Calculations of response of 5″ and 8″ Bonner Sphere detector.

Energy	5″ Bonner Sphere (126.70 cm²)[a]			8″ Bonner Sphere (324.30 cm²)[a]		
	Counts[b]	Error (%)	Response[c] [cm²]	Counts[b]	Error (%)	Response[c] [cm²]
0.1 eV	—	—	—	—	—	—
0.6 eV	—	—	—	—	—	—
1 eV	—	—	—	—	—	—
10 eV	0.17	0.90	21.06	0.01	9.95	3.12
100 eV	—	—	—	—	—	—
1 keV	0.23	0..82	29.06	0.02	7.50	6.50
10 keV	—	—	—	—	—	—
100 keV	—	—	—	0.04	5.80	13.21
500 keV	—	—	—	0.07	1.10	21.90
750 keV	—	—	—	—	—	—
1 MeV	0.21	0.84	26.52	0.08	2.96	27.17
2 MeV	—	—	—	0.09	0.73	29.31
10 MeV	—	—	—	—	—	—
20 MeV	—	—	—	—	—	—
GRN	0.19	1.35	24.07	0.08	2.13	26.05
FFTB	0.16	0.49	19.79	0.04	0.87	14.20

[a] cross sectional area of the detector

[b] number of reactions per source neutron in LiI

[c] per unit fluence

57

Table 3. MCNP Calculations of response of 10″ and 12″ Bonner Sphere detector.

Energy	10″ Bonner Sphere (506.7 cm²)[a]			12″ Bonner Sphere (729.7 cm²)[a]		
	Counts[b]	Error (%)	Response[c] [cm²]	Counts[b]	Error (%)	Response[c] [cm²]
0.1 eV	4.23E-04	15.10	0.21	—	—	—
0.6 eV	—	—	—	—	—	—
1 eV	1.23E-03	8.60	0.61	—	—	—
10 eV	—	—	—	—	—	—
100 eV	—	—	—	8.70E-04	9.60	0.63
1 keV	2.90E-03	5.90	1.47	1.02E-03	8.20	0.74
10 keV	—	—	—	—	—	—
100 keV	—	—	—	—	—	—
500 keV	2.01E-02	1.70	10.16	7.93E-03	4.90	5.78
750 keV	—	—	—	—	—	—
1 MeV	3.20E-02	2.06	16.21	1.44E-02	2.90	10.51
2 MeV	4.41E-02	1.20	1.20	2.44E-02	3.60	17.83
10 MeV	—	—	—	—	—	—
20 MeV	—	—	—	—	—	—
GRN	4.50E-02	4.20	22.80	2.12E-02	5.10	15.47
FFTB	1.96E-02	1.61	9.91	9.76E-03	1.85	7.12

a cross sectional area of the detector

b number of reactions per source neutron in LiI

c per unit fluence

58

4.2 Measurements and comparisons

The measurements for the arrival time distributions were made for the moderated BF_3 detector, AB remmeter, 2″ and 10″ Bonner Sphere detectors. The results are shown in Figs. 4.9 - 4.12, respectively. The integral plots were used for this analysis. The measurement results are compared with the corresponding integral plots of the calculated neutron arrival time distributions (i.e. MCNP calculated fractional cumulative counts for measured FFTB spectrum).

Figure. 4.9a and b shows the comparison between the measured and calculated results for the moderated BF_3 detector. In this figure, calculation results include the FFTB measured neutron spectrum and the MCNP-calculated GRN spectra with three different values of parameter 'a' (a = 1 MeV, 1.2 MeV, 0.8 MeV). The MCNP calculation results for different spectra are very similar. The measurements (for the FFTB measured neutron spectrum) differ from calculations by ≈ 20% at 100 μs. The error in both calculation and measurements are less than 2%.

Figure 4.10a and b shows the comparison between measurement and calculation results for an AB remmeter. There is a difference of ≈ 15% at 100 μs. The statistical error in both calculations as well as measurements are less than 1.5%. The discrepancies in the moderated BF_3 detector and AB remmeter comparison are real and unexplained at present, which need further investigation.
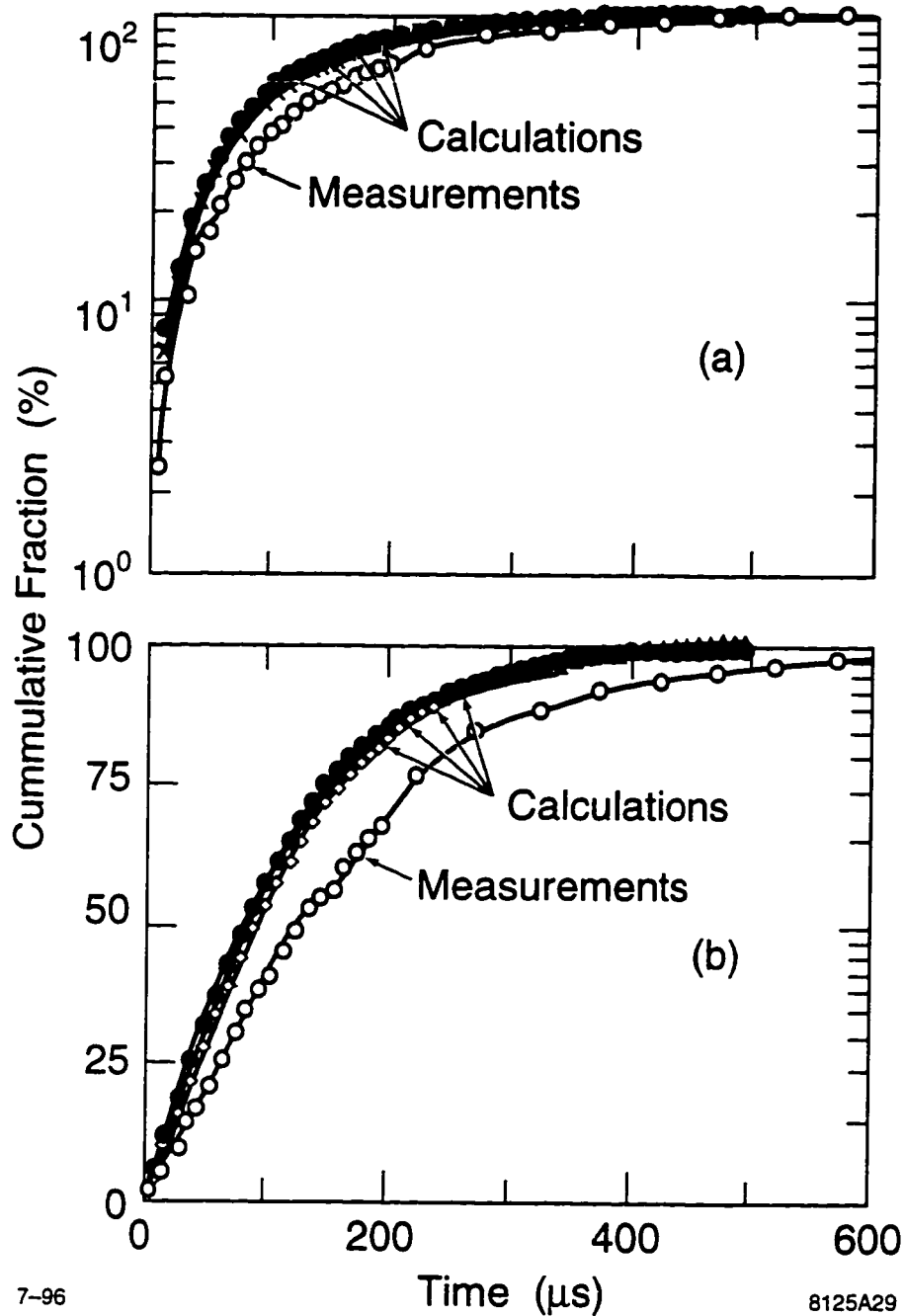
Figs. 4.9a and b A comparison between the MCNP-calculations and the measurement of fractional cumulative counts versus the neutron arrival time for the FFTB spectrum incident on the moderated BF₃ detector (a) a semilog plot (b) a linear plot. The calculations include the results for three GRN spectra (for a =1 MeV, a =1.2 MeV, and a =0.8 MeV) and the measured FFTB neutron spectrum.
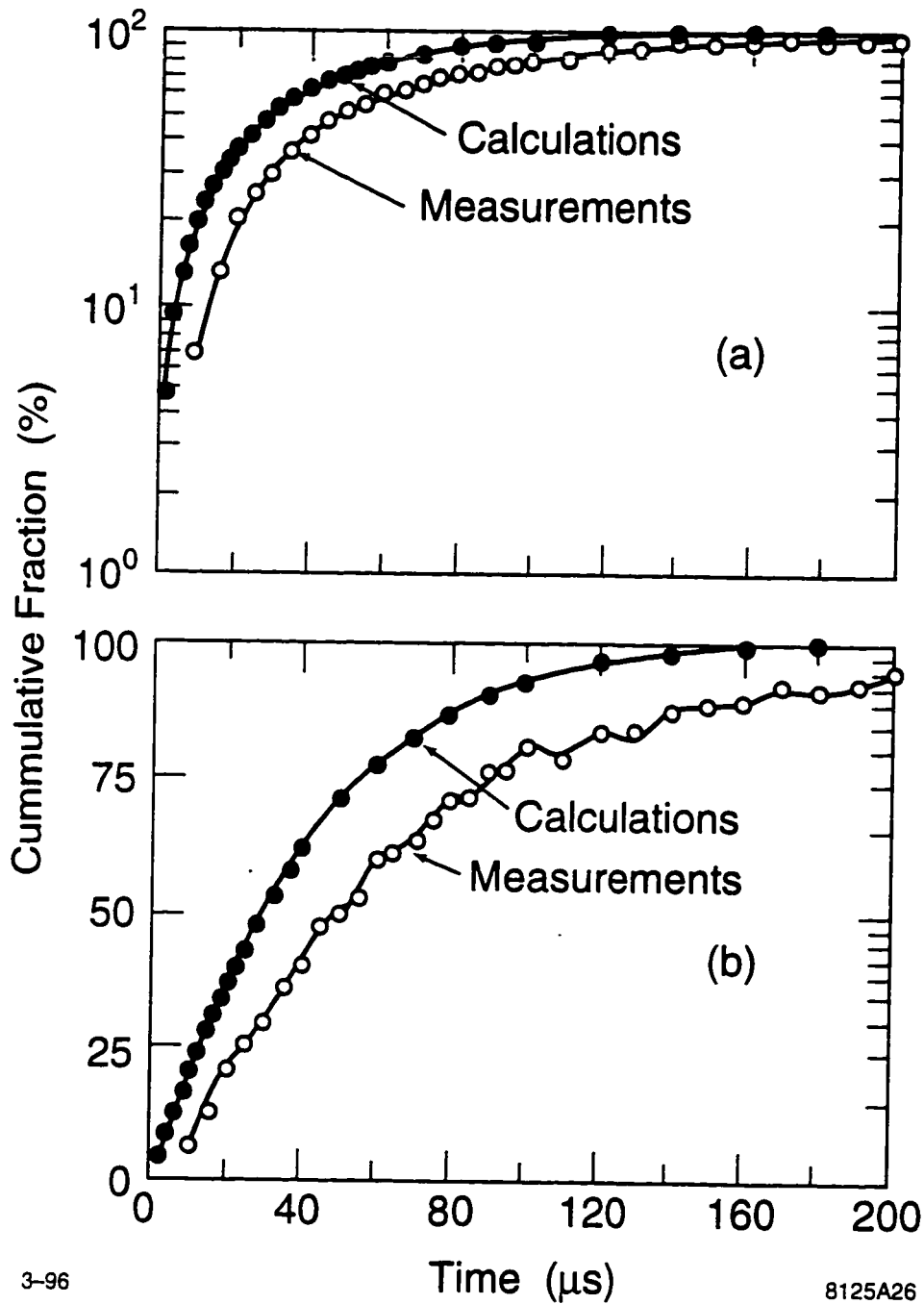
Figs. 4.10a and b A comparison between the MCNP-calculations and the measurement of fractional cumulative counts versus the neutron arrival time for the FFTB spectrum incident on the <u>Anderson-Braun remmeter</u> (a) a semilog plot (b) a linear plot.
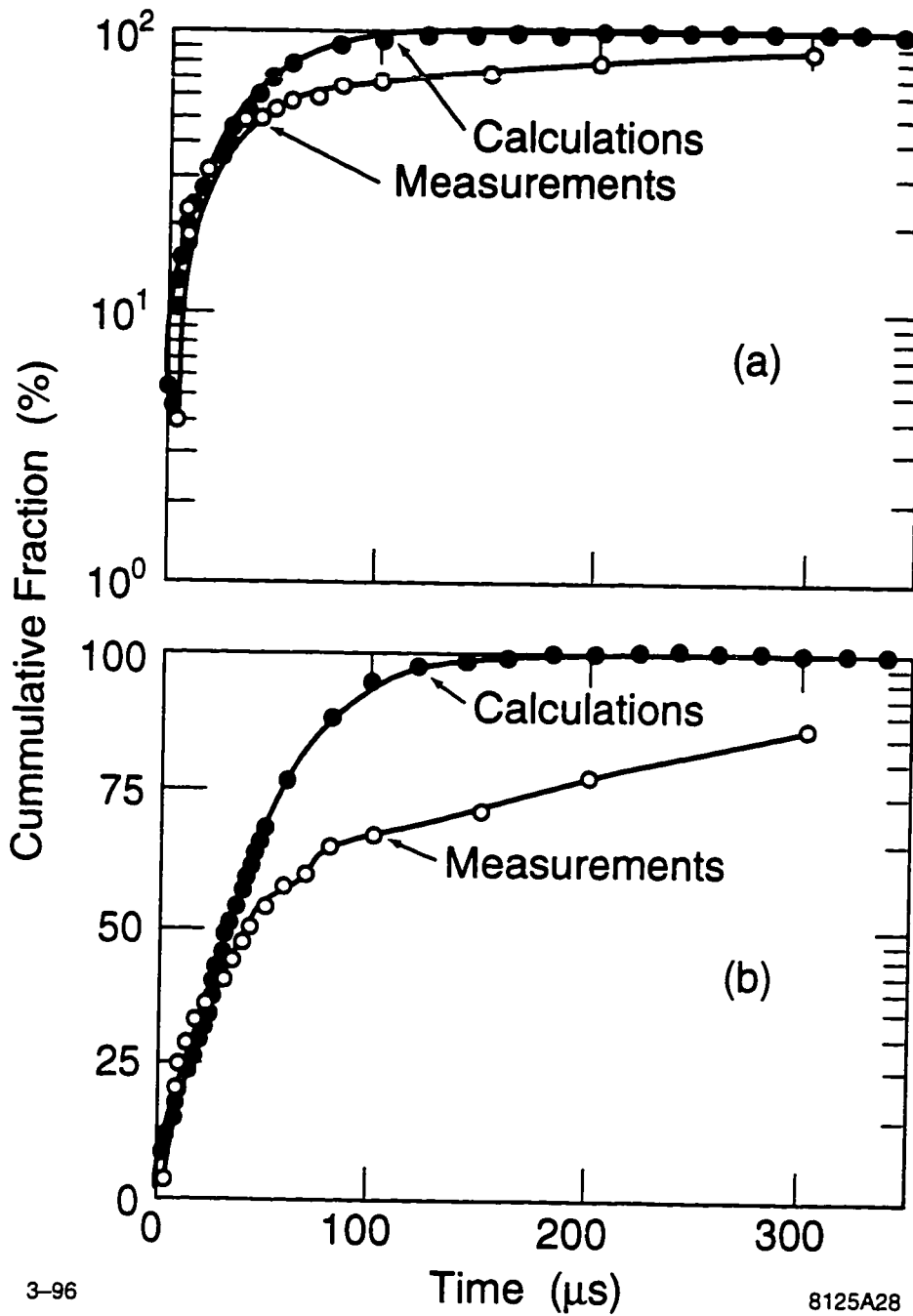
Figs. 4.11a and b A comparison between the MCNP-calculations and the measurement of fractional cumulative counts versus the neutron arrival time for the FFTB spectrum incident on the 2" Bonner Sphere detector (a) a semilog plot (b) a linear plot.
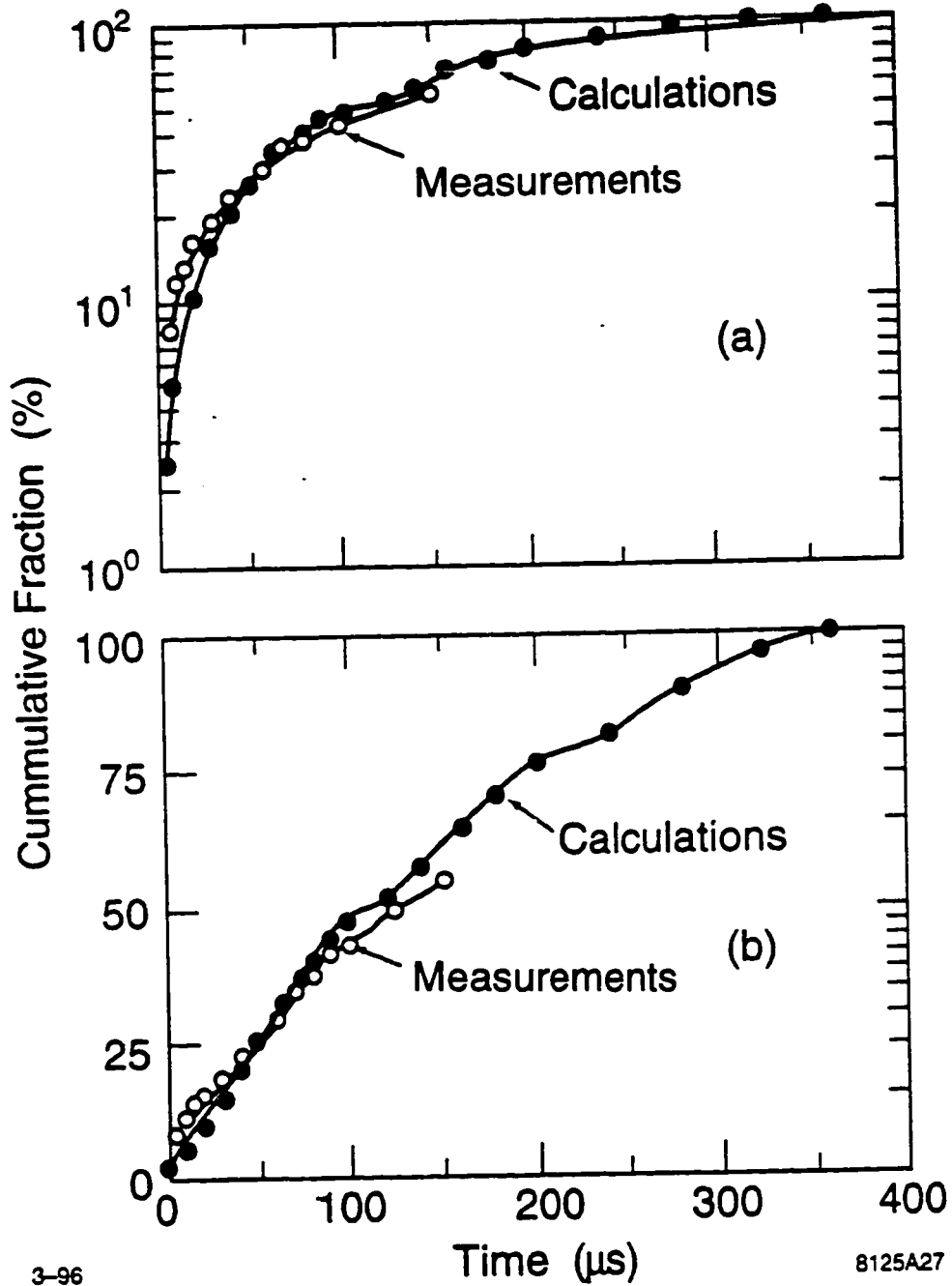
Figs. 4.12a and b A comparison between the MCNP-calculations and the measurement of fractional cumulative counts versus the neutron arrival time for the FFTB spectrum incident on the 10″ Bonner Sphere detector (a) a semilog plot (b) a linear plot.

Figure 4.11a and b is a comparison between the calculations and measurements for 2″ Bonner Sphere detector. It is clear that the 2″ Bonner Sphere calculations reach to 100% much faster than the measurement result. This can be explained by the fact that the 2″ Bonner Sphere is most sensitive to low energy neutrons and, in the real case, low energy neutrons in FFTB spectrum are delayed by the timing effect of concrete shielding before they reach the detector. In the calculations, this shielding effect is not accounted for. If this delay of slow neutrons is simulated in MCNP calculation, the results would agree better with the measurements.

A comparison in the calculations and measurements results for the 10″ Bonner Sphere detector is shown in Fig. 4.12a and b. The calculation results are in close agreement with the measurement.

4.3 Calculation of T-values

The mean arrival time (T-value) is the inverse of the slope of the neutron arrival time distributions. T-values for various detectors have been calculated for FFTB spectrum from the calculated neutron arrival time distributions and are shown in the Table 4.

Table 4. Mean neutron arrival time for FFTB spectrum

Detector	T-value (μs)
BF$_3$ detector	107
AB remmeter	43
Bonner Spheres	
2″	25
3″	83
5″	126
8″	205
10″	241
12″	259

5. SUMMARY AND CONCLUSIONS

5.1 Summary

Neutron arrival time distributions for three moderating type fast neutron detectors were calculated using the MCNP4A code. The detectors were a moderated BF_3 detector, an Anderson-Braun remmeter and Bonner Sphere detectors (of 2″, 3″, 5″, 8″, 10″, and 12″ diameter). Each of the detectors had polyethylene as a moderator.

The input files including modeled geometry of each detector and various source descriptions were developed. Number of reactions in the sensor per source neutron as a function of neutron arrival time was calculated. Output from the MCNP code was represented as the neutron arrival time distributions. The response of each detector was also calculated. Results obtained were discussed for each detector.

The results from the calculations were compared with the measurement made at FFTB (46.7 GeV e⁻ beam dump at SLAC) for the moderated BF_3 detector, AB remmeter and Bonner Spheres (of 2″ and 10″ diameter).

The calculated and measured results for large Bonner Sphere (10″) are in close agreement. The disagreement for 2″ Bonner Sphere is due the delay in low-energy neutrons before they reach the detector. The delay is introduced by the timing effect of the concrete shielding, which was not accounted for in the MCNP calculations.

The difference in the measured and calculated results for the moderated BF_3 detector and AB remmeter can not be completely explained at present.

5.2 Conclusions

From the study of the MCNP calculated neutron arrival time distributions of

moderating type detectors, the following conclusions can be drawn:

1) The neutron arrival time distributions exhibit the exponential behavior

2) For each detector in this study there is a noticeable shift in the peak of the neutron

arrival time distributions, depending on the thickness of the moderator and the energy of

the incident neutrons. The delay in the arrival of low-energy incident neutrons at the

sensor is due to low-energy neutrons becoming thermalized near the surface of the

detector. The thermal neutrons in this case have to diffuse through a larger moderator

thickness to reach the sensor as compared to the case of fast incident neutrons

3) The neutron arrival time distributions are spectrum dependent.

4) The neutron arrival time distributions for Bonner Spheres (LiI sensor) detectors

show a spike at the beginning of the curve. It might be partially explained by the presence

of pronounced response peak around 250 keV in the cross section of ^{6}Li(n, α)^{3}H reaction.

5) The MCNP calculated responses of all detectors are reasonable and have the shapes

as expected. The moderated BF$_3$ detector has a peak at 1 MeV. AB remmeter has a peak

at about 2 MeV. The Bonner Sphere detectors of small diameters (2″, 3″, and 5″) have

high response to low energy incident neutron and larger spheres (8″, 10″, and 12″) have

high response to high energy incident neutrons.

6) Except for the 2″ and 3″ Bonner Sphere all the detectors show lower response to

the FFTB measured spectrum than GRNs and 1 MeV monoenergetic neutrons.

The 10″ Bonner Sphere detector shows a good agreement between the measured and calculated results. The comparison of 2″ Bonner Sphere calculations and the measurements results shows discrepancies. The calculations show that neutrons reach the detector faster than that of the measurement results.

Similar calculations were done by Liu (1996) for an experimental setup at ANL (Argonne National Laboratory). He simulated the ANL room geometry with MCNP for 2″ Bonner Sphere detector. The timing effect of the concrete shielding was also incorporated in the calculations. The arrival time distribution results closely agree with the experimental data for that set-up.

Therefore, the discrepancies of 2″ Bonner Sphere detector for our work may be explained by the fact that the low-energy neutrons are significantly delayed through the concrete shielding in FFTB dump before entering the detector. This effect was not accounted for in our calculations and therefore, the calculated 2″ sphere results do not agree with the measurements.

The comparison between the measured and calculated results for AB remmeter and moderated BF_3 detector show discrepancies and can not be completely explained at present. However, it can be postulated that it may be due to the anisotropic response of these detectors. The measurements include neutrons incident from all sides, whereas in the calculations, neutron sources are simulated as incident only in the direction perpendicular to the detector axis. The neutrons incident parallel to the detector axis could have longer arrival time and can reach the sensor later in time as found in the measurements. Further studies are needed for the confirmation of this postulate.

5.3 Further studies

The first further work would be the calculation of the timing effect of the concrete

shielding and its effect on the arrival of neutrons in various detectors. Another study

would be to calculate the slopes (and therefore, T-values) of the neutron arrival time

distributions for various detectors for other spectra. This could be helpful in the

calculations of the dead time correction factor for moderating type fast neutron detectors

operating in pulse mode in a pulsed radiation field.

REFERENCES

Ash, W.; DeStaebler, H.; Harris, J.; and Murray, J. PEP radiation shielding tests in SLAC A Beam. SLAC-TN-77-5, PEP-252, Stanford Linear Accelerator Center, Stanford, CA; 1977.

International Commission on Radiological Protection. Data for protection against ionizing radiation for external sources. Oxford Pergamon Press, ICRP Publication 21; 1973.

International Atomic Energy Agency. Radiation safety aspects of the operation of electron linear accelerators. Technical report series no. 188, IAEA Vienna; 1979.

Jenkins, T.M. Neutron and photon measurements through concrete from a 15 GeV electron beam on a target - comparison with model and calculations. Nucl. Instrum. Methods 159, pp. 265-288 (1979).

Knoll, G.F. Radiation detection and measurement. 2nd edition, John Wiley & Son, Inc.; 1989.

Kosako, T.; Nakamura, T.; Iwai, S. Estimation of response function of moderating type neutron detectors by the time-of-flight method combined with a large lead pile. Nucl. Instrum. Methods in Phys. Res., A235, pp. 103-122; 1985.

Liu, J. C.; Jenkins, T. M; McCall, R. C.; Ipe, N. E. Neutron dosimetry at SLAC: neutron sources and instrumentation. Report No. SLAC-TN-91-3 Stanford Linear Accelerator Center, Stanford, CA; 1991.

Liu, J.C. Private communications. SLAC; 1996.

MCNP - A General purpose Monte Carlo N-Particle Transport Code, Version 4A, Los Alamos National Laboratory, New Mexico; 1993.

Patterson, H. W; Thomas, R. H. Accelerator health physics. Academic press, Inc. New York, NY (1973).

Rokni, S. Private communications. SLAC; 1996.

Thai, X. Private communication. SLAC; 1996.

Appendix A1

MCNP input file of the moderated BF₃ detector for monoenergetic neutrons (20 MeV).

```
     Neutron moderation time in detectors                    JLiu0594
C SLAC moderated BF3 (RS-P1-1613-114 model)
1      1 -0.002567    -1 10 -11                   $ BF3 gas (70 cmHg)
2      2 -2.70        -1 11 -14                   $ Al preAmp
3      2 -2.70        1 -2 10 -14                 $ Al wall for BF3 tube
4      2 -2.70        -2 9 -10                    $ Al bottom of tube
5      3 -0.95        (2 -3 8 -12):(-2 8 -9)      $ PE
6      4 -8.65        (3 -4 7 -13):(-3 7 -8)      $ bottom and side Cd
7      4 -8.65        2 -3 12 -13                 $ top Cd
8      2 -2.70        (4 -5 6 -14):(-4 6 -7)      $ bottom and side Al
9      2 -2.70        2 -4 13 -14                 $ top Al
10     0              ((5:-6:14)-16 15):(-16 -15) $ outer void
11     0              16

1      cz  2.5              $ ID of BF3 sensitive radius
2      cz  2.55             $ OD of tube Al wall (0.05 cm thick)
3      cz  8.55             $ OD of PE moderaotr (6 cm thick)
4      cz  8.63             $ OD of Cd surrounding (0.08 cm thick)
5      cz  9.33             $ OD of Al case (0.7 cm thick)
6      pz  0.0              $ bottom plane of Al case
7      pz  0.7              $ bottom of Cd
8      pz  0.78             $ bottom of PE
9      pz  6.78             $ bottom of BF3 Al tube
10     pz  6.83             $ bottom of BF3 gas plane
11     pz  37.83            $ top of BF3 gas plane (31 cm long)
12     pz  43.28            $ top of Cd
13     pz  43.36            $ top of Al
14     pz  44.06            $ top plane of Al case
15     py  -10              $ source surface
16     sz  22.03   200      $ outer surface

mode   n                    $ neutron time-dependent problem
C importance and discard
imp:n  1 1 1 1 1 1 1 1 1 1 0
C monoenergy neutron incident parallel on moderator surface
sdef   erg=20.0 sur=15 pos=0 -10 22.03  x=d1 z=d2 y=-10 vec=0 1 0 &
       dir=1 tme=0
si1    -9.33 9.33
si2    0 44.06
sp1    0 1
sp2    0 1
C Score thermal neutron arrival time to the BF3
f4:n   1
fm4:n  -0.24 1 107
t4      1000  2000  3000  4000  5000  6000  7000  8000  9000 10000 &
       11000 12000 13000 14000 15000 16000 17000 18000 19000 20000 &
       21000 22000 23000 24000 25000 26000 27000 28000 29000 30000 &
       31000 32000 33000 34000 35000 36000 37000 38000 39000 40000 &
       41000 42000 43000 44000 45000 46000 47000 48000 49000 50000
m1     5010.50c 24 5011.55c 1 9019.50c 75   $ BF3 (96% B-10)
m2     13027.50c 1                          $ Al
m3     1001.50c 2 6000.50c 1                $ CH2 Polyethylene
mt3    poly.01t                             $ S table for PE
m4     48000.50c 1                          $ Cd
C VOID
C phys:n emax=20 emcnf=20       $ A CARD TO CHECK GEOMETRY ONLY
cut:n 50000 1.0E-9
nps    1000000
print  50 110
```

Appendix A2

MCNP input file of the moderated BF₃ detector for GRNs.

```
Neutron moderation time in detectors              JLiu0594
C SLAC moderated BF3 (RS-P1-1613-114 model)
1     1 -0.002567    -1 10 -11           $ BF3 gas (70 cmHg)
2     2 -2.70        -1 11 -14           $ Al preAmp
3     2 -2.70        1 -2 10 -14         $ Al wall for BF3 tube
4     2 -2.70        -2 9 -10            $ Al bottom of tube
5     3 -0.95        (2 -3 8 -12):(-2 8 -9)    $ PE
6     4 -8.65        (3 -4 7 -13):(-3 7 -8)    $ bottom and side Cd
7     4 -8.65        2 -3 12 -13         $ top Cd
8     2 -2.70        (4 -5 6 -14):(-4 6 -7)    $ bottom and side Al
9     2 -2.70        2 -4 13 -14         $ top Al
10    0              ((5:-6:14)-16 15):(-16 -15) $ outer void
11    0              16

1     cz 2.5                    $ ID of BF3 sensitive radius
2     cz 2.55                   $ OD of tube Al wall (0.05 cm thick)
3     cz 8.55                   $ OD of PE moderaotr (6 cm thick)
4     cz 8.63                   $ OD of Cd surrounding (0.08 cm thick)
5     cz 9.33                   $ OD of Al case (0.7 cm thick)
6     pz 0.0                    $ bottom plane of Al case
7     pz 0.7                    $ bottom of Cd
8     pz 0.78                   $ bottom of PE
9     pz 6.78                   $ bottom of BF3 Al tube
10    pz 6.83                   $ bottom of BF3 gas plane
11    pz 37.83                  $ top of BF3 gas plane (31 cm long)
12    pz 43.28                  $ top of Cd
13    pz 43.36                  $ top of Al
14    pz 44.06                  $ top plane of Al case
15    py -10                    $ source surface
16    sz 22.03   200            $ outer surface

mode    n                $ neutron time-dependent problem
C importance and discard
imp:n  1 1 1 1 1 1 1 1 1 1 0
C GRN incident parallel on moderator surface
sdef    erg=d3 sur=15 pos=0 -10 22.03  x=d1 z=d2 y=-10 vec=0 1 0 &
        dir=1 tme=0
si1    -9.33 9.33
si2    0 44.06
sp1    0 1
sp2    0 1
sp3    -5 1.0        $ evaporaton spectrum, a=1.0mev
C Score thermal neutron arrival time to the BF3
f4:n   1
fm4:n  -0.24 1 107
t4      1000  2000  3000  4000  5000  6000  7000  8000  9000 10000 &
       11000 12000 13000 14000 15000 16000 17000 18000 19000 20000 &
       21000 22000 23000 24000 25000 26000 27000 28000 29000 30000 &
       31000 32000 33000 34000 35000 36000 37000 38000 39000 40000 &
       41000 42000 43000 44000 45000 46000 47000 48000 49000 50000
m1     5010.50c 24 5011.55c 1 9019.50c 75    $ BF3 (96% B-10)
m2     13027.50c 1                    $ Al
m3     1001.50c 2 6000.50c 1          $ CH2 Polyethylene
mt3    poly.01t                       $ S table for PE
m4     48000.50c 1                    $ Cd
C VOID                        $ A CARD TO CHECK GEOMETRY ONLY
C phys:n emax=20 emcnf=20
cut:n 50000 1.0E-9
nps    1000000
print  50 110
```

71

Appendix A3

MCNP input file of the moderated BF₃ detector for FFTB measured neutron spectrum.

```
Neutron moderation time in detectors                    JLiu0594
C SLAC moderated BF3 (RS-P1-1613-114 model)
1      1 -0.002567   -1 10 -11            $ BF3 gas (70 cmHg)
2      2 -2.70       -1 11 -14            $ Al preAmp
3      2 -2.70       1 -2 10 -14          $ Al wall for BF3 tube
4      2 -2.70       -2 9 -10             $ Al bottom of tube
5      3 -0.95       (2 -3 8 -12):(-2 8 -9)   $ PE
6      4 -8.65       (3 -4 7 -13):(-3 7 -8)   $ bottom and side Cd
7      4 -8.65       2 -3 12 -13          $ top Cd
8      2 -2.70       (4 -5 6 -14):(-4 6 -7)   $ bottom and side Al
9      2 -2.70       2 -4 13 -14          $ top Al
10     0             ((5:-6:14)-16 15):(-16 -15) $ outer void
11     0             16

1      cz   2.5              $ ID of BF3 sensitive radius
2      cz   2.55             $ OD of tube Al wall (0.05 cm thick)
3      cz   8.55             $ OD of PE moderaotr (6 cm thick)
4      cz   8.63             $ OD of Cd surrounding (0.08 cm thick)
5      cz   9.33             $ OD of Al case (0.7 cm thick)
6      pz   0.0              $ bottom plane of Al case
7      pz   0.7              $ bottom of Cd
8      pz   0.78             $ bottom of PE
9      pz   6.78             $ bottom of BF3 Al tube
10     pz   6.83             $ bottom of BF3 gas plane
11     pz   37.83            $ top of BF3 gas plane (31 cm long)
12     pz   43.28            $ top of Cd
13     pz   43.36            $ top of Al
14     pz   44.06            $ top plane of Al case
15     py   -10              $ source surface
16     sz   22.03   200      $ outer surface

mode   n                     $ neutron time-dependent problem
C importance and discard
imp:n  1 1 1 1 1 1 1 1 1 1 0
C FFTB hot spectrum  parallel on moderator surface
sdef   erg=d1 sur=15 pos=0 -10 22.03  x=d2 z=d3 y=-10 vec=0 1 0 &
       dir=1 tme=0
si1         0  0.000000414  0.0000006826  0.000001445  0.000003059 &
       0.000006476  0.00001371  0.00002902  0.00006144  0.0001301 &
       0.0002754  0.0005929  0.001234  0.002613  0.005531 &
       0.01171  0.02479  0.05247  0.1111  0.2237 &
       0.4508  0.9072  1.872  3.679  7.408 &
       14.92  20.0
sp1  c          0  108000  116124  126794  136239 &
          144998  153349  161496  169655  177999 &
          186716  196147  205821  216541  228281 &
          241361  256131  273241  294101  319331 &
          353621  398511  454501  505971  554621 &
          600031  618431
si2    -9.33 9.33
si3    0 44.06
sp2    0 1
sp3    0 1
C Score thermal neutron arrival time to the BF3
f4:n   1
fm4:n  -0.24 1 107
t4     1000   2000   3000   4000   5000   6000   7000   8000   9000 10000 &
       11000 12000 13000 14000 15000 16000 17000 18000 19000 20000 &
       21000 22000 23000 24000 25000 26000 27000 28000 29000 30000 &
       31000 32000 33000 34000 35000 36000 37000 38000 39000 40000 &
       41000 42000 43000 44000 45000 46000 47000 48000 49000 50000
m1     5010.50c 24 5011.55c 1 9019.50c 75     $ BF3 (96% B-10)
m2     13027.50c 1                            $ Al
m3     1001.50c 2 6000.50c 1                  $ CH2 Polyethylene
mt3    poly.01t                               $ S table for PE
m4     48000.50c 1                            $ Cd
C VOID                        $ A CARD TO CHECK GEOMETRY ONLY
C phys:n emax=20 emcnf=20
cut:n 50000 1.0E-9
nps    1000000
print  50 110
```

Appendix B1

MCNP input file of the Anderson-Braun remmeter for monoenergetic neutrons (1 MeV).

```
Neutron moderation time in detectors              rka1095
C SLAC moderated AB detector
1      1 -0.002567   -1 8 -9              $ BF3 gas (70 cmHg)
2      2 -2.70       -1 9 -12            $ Al preAmp
3      3 -0.95        (-2 1 7 -10):(-1 7 -8)   $ PE
4      4 -0.78           6 -7 -3             $ bottom of boron cyl
5      4 -0.78           7 2 -3 -10          $ sides of boron cyl.
6      4 -0.78           1 -3 10 -11         $ top of boron plastic cyl.
7      3  -0.95     (-4 3 5 -12):(-3 5 -6)   $ outer PE
8      3  -0.95     -3 1 11 -12             $ outer PE
9      0           (4 :-5 :12)-14           $ inner vac.
10     0           14                       $ outer world

1      cz   1.7
2      cz   3.3
3      cz   3.8
4      cz   10.3
5      pz   0.0
6      pz   4.6
7      pz   5.1
8      pz   6.7
9      pz   17.5
10     pz   19.1
11     pz   19.6
12     pz   24.2
13     py   -11
14     sz   12.1   200

mode   n                      $ neutron time-dependent problem
C importance and discard
imp:n  1 8R 0
C monoenergy neutron incident parallel on moderator surface
sdef    erg=1.0 sur=13 pos=0 -11 12.1  x=d1 z=d2 y=-11 vec=0 1 0 &
        dir=1 tme=0
si1     -10.33 10.33                    .
si2     0 24.2
sp1     0 1
sp2     0 1
C Score thermal neutron arrival time to the BF3
f4:n   1
fm4:n  -0.24 1 107
t4        200    400    600    800    1000 &
         1200   1400   1600   1800    2000 &
         2400   2800   3200   3600    4000  5000   6000 &
         7000  8000   9000 10000 12000 14000 16000 18000  20000
m1      5010.50c 24 5011.55c 1 9019.50c 75     $ BF3 (96% B-10)
m2      13027.50c 1                    $ Al
m3      1001.50c 2 6000.50c 1          $ CH2 Polyethylene
mt3     poly.01t                       $ S table for PE
m4      1001.50c 64 6000.50c 31 5010.50c 5   $ boron plastic
C VOID                                 $TO CHECK GEOMETRY
C phys:n emax=20 emcnf=20
cut:n  20000 1.0E-9
nps    10000000
print  50 110
```

Appendix B2

MCNP input file of the Anderson-Braun remmeter for GRNs.

```
>Neutron moderation time in detectors            rka1095
C SLAC moderated AB detector
1     1 -0.002567   -1 8 -9              $ BF3 gas (70 cmHg)
2     2 -2.70       -1 9 -12             $ Al preAmp
3     3 -0.95       (-2 1 7 -10):(-1 7 -8)  $ PE
4     4 -0.78        6 -7 -3                 $ bottom of boron cyl
5     4 -0.78        7 2 -3 -10              $ sides of boron cyl.
6     4 -0.78        1 -3 10 -11             $ top of boron plastic cyl.
7     3 -0.95       (-4 3 5 -12):(-3 5 -6)   $ outer PE
8     3 -0.95       -3 1 11 -12              $ outer PE
9     0             (4 :-5 :12)-14           $ inner vac.
10    0              14                      $ outer world

1     cz   1.7
2     cz   3.3
3     cz   3.8
4     cz   10.3
5     pz   0.0
6     pz   4.6
7     pz   5.1
8     pz   6.7
9     pz   17.5
10    pz   19.1
11    pz   19.6
12    pz   24.2
13    py  -11      .
14    sz   12.1  200

mode   n                     $ neutron time-dependent problem
C importance and discard
imp:n  1 8R 0
C GRN incident parallel on moderator surface
sdef    erg=d3 sur=13 pos=0 -11 12.1  x=d1 z=d2 y=-11 vec=0 1 0 &
        dir=1 tme=0
si1    -10.33 10.33
si2     0 24.2
sp1     0 1
sp2     0 1
sp3    -5 1.0     $ evaporaton spectrum. a=1.0mev
C Score thermal neutron arrival time to the bf3
f4:n   1
fm4:n  -0.24 1 107
t4         200    400    600    800    1000 &
          1200   1400   1600   1800    2000 &
          2400   2800   3200   3600    4000   5000    6000 &
          7000   8000   9000  10000   12000  14000  16000  18000   20000
m1     5010.50c 24 5011.55c 1 9019.50c 75    $ BF3 (96% B-10)
m2     13027.50c 1                           $ Al
m3     1001.50c 2 6000.50c 1                 $ CH2 Polyethylene
mt3    poly.01t                              $ S table for PE
m4     1001.50c 64 6000.50c 31 5010.50c 5    $ boron plastic
C VOID                                       $TO CHECK GEOMETRY
C phys:n emax=20 emcnf=20
cut:n  20000 1.0E-9
nps    10000000
print  50 110
```

Appendix B3

MCNP input file of the Anderson-Braun remmeter for FFTB measured neutron spectrum

```
Neutron moderation time in detectors              rka1095
C SLAC moderated AB detector
1      1 -0.002567   -1 8 -9            $ BF3 gas (70 cmHg)
2      2 -2.70        -1 9 -12          $ Al preAmp
3      3 -0.95         (-2 1 7 -10):(-1 7 -8)   $ PE
4      4 -0.78              6 -7 -3       $ bottom of boron cyl
5      4 -0.78              7 2 -3 -10    $ sides of boron cyl.
6      4 -0.78              1 -3 10 -11   $ top of boron plastic cyl.
7      3 -0.95         (-4 3 5 -12):(-3 5 -6)    $ outer PE
8      3 -0.95         -3 1 11 -12        $ outer PE
9      0               (4 :-5 :12)-14     $ inner vac.
10     0               14                 $ outer world

1      cz   1.7
2      cz   3.3
3      cz   3.8
4      cz   10.3
5      pz   0.0
6      pz   4.6
7      pz   5.1
8      pz   6.7
9      pz   17.5
10     pz   19.1
11     pz   19.6
12     pz   24.2
13     py   -11
14     sz   12.1  200

mode   n                      $ neutron time-dependent problem
C importance and discard
imp:n  1 8R 0
C FFTB hot spectrum  parallel on moderator surface
sdef   erg=d1 sur=13 pos=0 -11 12.1  x=d2 z=d3 y=-11 vec=0 1 0 &
       dir=1 tme=0
si1    0  0.000000414  0.0000006826  0.000001445  0.000003059 &
       0.000006476  0.00001371  0.00002902  0.00006144  0.0001301 &
       0.0002754  0.0005929  0.001234  0.002613  0.005531 &
       0.01171  0.02479  0.05247  0.1111  0.2237 &
       0.4508  0.9072  1.872  3.679  7.408 &
       14.92  20.0
sp1  C          0  108000  116124  126794  136239 &
       144998  153349  161496  169655  177999 &
       186716  196147  205821  216541  228281 &
       241361  256131  273241  294101  319331 &
       353621  398511  454501  505971  554621 &
       600031  618431
si2    -10.33 10.33
si3    0 24.2
sp2    0 1
sp3    0 1
C Score thermal neutron arrival time to the BF3
f4:n   1
fm4:n  -0.24 1 107
t4        200    400    600    800    1000 &
         1200   1400   1600   1800   2000 &
         2400   2800   3200   3600   4000  5000   6000 &
         7000 8000   9000 10000 12000 14000 16000 18000  20000
m1     5010.50c 24 5011.55c 1 9019.50c 75    $ BF3 (96% B-10)
m2     13027.50c 1                           $ Al
m3     1001.50c 2 6000.50c 1                 $ CH2 Polyethylene
mt3    poly.01t                              $ S table for PE
m4     1001.50c 64 6000.50c 31 5010.50c 5    $ boron plastic
C VOID                                       $TO CHECK GEOMETRY
C phys:n emax=20 emcnf=20
cut:n  20000 1.0E-9
nps    10000000
print  50 110
```

Appendix C1

MCNP input file of the 2″ Bonner Sphere for monoenergetic neutrons (1 MeV).

```
2' Bonner sphere with LiJ detector (no Iodine, no lead) for timing
C   JLIU 100995 (modified from VV/11.1.94)
1     0          1                                        $ Outer void
2     0          -1 2:-2 7 3:-2 -7 3 24:-2 -7 -23:-6 -2  $ Inner void
3     0          -3 24 4:16 4 -3 -24    $ PE1 - outmost
4     0          -3 -24 21 9 4 -16      $ PE2
5     1  -0.955  -5 20                  $ PE4
6     1  -0.955  -5 16 -20              $ PES - above LiJ in 5
C   ------- LEAD, POLY OR VACUUM LAYER ---------
7     0          (-4 5 29):(-4 5 -29 11 20) $ Pb-1 upper part
8     0          -11 -4 5 10 26            $ Pb-2 mid part with cone
9     0          -4 -10 21                 $ Pb-3 lowest part
C   ----------------------------------
10    3  -2.6989  -24 23 -9 6:-9 7 -23 22   $ AL-1 starting from bottom
11    3  -2.6989  -9 8 -22 19              $ AL-2
12    3  -2.6989  -10 9 -21 19             $ AL-3
13    3  -2.6989  -11 10 -26 25            $ AL-4 conical transition
14    3  -2.6989  -16 11 -20 18:-16 15 -18 $ AL-5 top part
15    3  -2.6989  -14 13 -18:-13 12 -18 17 $ AL-6 around detector
C   ----------------------------------
16    4  -2.2     -12 27 -18              $ Glass
17    5   0.01655 -13 12 -17             $ 6-Li in atx1.E-24/cm3
C   ----------------------------------
18    6  -1.19    -27 11 -18             $ Plexi-1 starting from top
19    6  -1.19    -11 10 -25             $ Plexi-2 conical shape
20    6  -1.19    -10 7 -19              $ Plexi-3
21    6  -1.19    -8 7 -22 19            $ Plexi-4
22    0           -15 14 -18             $ Sponge - neglected

1     SO   1000.0       $ Sphere for the black hole
2     SO     50.0       $ Vacuum sphere (want same order as in FLUKA)
3     SO   15.24        $ 12' sphere
4     SO    5.001       $ 10 cm lead sphere
5     SO    2.54        $ 1.0' RADIUS inner PE sphere
6     PZ  -20.0         $ Bottom of scint. probe
7     PZ  -10.782       $ End PM. start plexi
8     PZ  -10.465       $ End large plexi disc
9     PZ   -9.512       $ End large Al tube
10    PZ   -4.051       $ Start conical transition
11    PZ   -3.670       $ End conical transition
12    PZ   -0.200       $ Bottom of LiJ crystal
13    PZ    0.200       $ Top of LiJ crystal
14    PZ    0.274       $ Top Al housing of LiJ crystal
15    PZ    0.490       $ Top of sponge above crystal
16    PZ    0.710       $ Top of Al probe housing
17    CZ    0.200       $ LiJ crystal
18    CZ    0.556       $ Inside top part of probe
19    CZ    0.655       $ Inside thicker part of probe
20    CZ    0.714       $ Out top part of probe
21    CZ    0.940       $ Outside thicker part of probe
22    CZ    1.295       $ End largest plexi
23    CZ    1.970       $ Inside PM Al housing tube
24    CZ    2.540       $ Outside PM Al housing tube
25    KZ   -1.5302424 0.06751814  -1   $ Inner cone
26    KZ   -2.4663097 0.35185759  -1   $ Outer cone
27    PZ   -0.537       $ Bottom of glass layer below LiJ
28    PX  -20.          $ Plane for the source
29    PZ   -2.43758     $ connection between sphere 5 and cylin. 20

mode    n
imp:n   0  1 20R
m1      1001.50c 2. 6000.50c 1.        $ Polyethylene
mt1     poly.01t                       $ Poly for thermals
m2      82000.50c 1.                   $ Lead
m3      13027.50c 1.                   $ Aluminum
m4      14000.50c 1. 8016.50c 2.       $ Glass SiO2
m5      3006.50c 1.0                   $ 6- Li
m6      6012.50c 2. 1001.50c 3. 8016.50c 1. $ C2HJO - plexi
c       1 MeV parallel neutron beam along x-axis
c       Uniform distribution
sdef    erg=1 par=1 sur=28 pos=-20 0 0 rad=d1 dir=1 tme=0
si1     2.54    $ Radius of plane circular monodir. source along x-axis
C scoring
f4:n    17
fm4     0.11733  5  105   $ multipler, material, reaction (n,t)
t4      200    400    600    800   1000  &
        1200   1400   1600   1800   2000  &
        2200   2400   2600   2800   3000  &
        3200   3400   3600   3800   4000  &
        4200   4400   4600   4800   5000  &
        6000   8000  10000  12000  14000  16000  18000  20000  22000  24000  &
        26000  28000  30000  32000  34000  36000  38000  40000  42000  44000  &
        46000  48000  50000
C phys:n  10.5  1.E-9  $ emax , emcnf : change emax dep. on source!!!
cut:n   50000 1.0E-9
prdmp   -30 -60
print   50 110
nps     10000000
```

76

Appendix C2

MCNP input file of the 8″ Bonner Sphere for GRNs.

```
1    0               1                                  $ Outer void
2    0              -1 2:-2 7 3:-2 -7 3 24:-2 -7 -23:-6 -2  $ Inner void
3    1   -0.955    -3 24 4:16 4 -3 -24        $ PE1 - outmost
4    1   -0.955    -3 -24 21 9 4 -16          $ PE2
5    1   -0.955    -5 11 20:-11 -5 26         $ PE4
6    1   -0.955    -5 16 -20                  $ PE5 - above LiJ in 5
c    ------- LEAD OR POLY LAYER ---------
7    1   -0.955    -4 5 11                    $ Pb-1 upper part
8    1   -0.955    -11 -4 5 10 26             $ Pb-2 mid part with cone
9    1   -0.955    -4 -10 21                  $ Pb-3 lowest part
c    -----------------------------------
10   3   -2.6989   -24 23 -9 6:-9 7 -23 22    $ AL-1 starting from bottom
11   3   -2.6989   -9 8 -22 19                $ AL-2
12   3   -2.6989   -10 9 -21 19               $ AL-3
13   3   -2.6989   -11 10 -26 25              $ AL-4 conical transition
14   3   -2.6989   -16 11 -20 18:-16 15 -18   $ AL-5 top part
15   3   -2.6989   -14 13 -18:-13 12 -18 17   $ AL-6 around detector
c    -----------------------------------
16   4   -2.2      -12 27 -18                 $ Glass
17   5   0.01655   -13 12 -17                 $ 6-Li in atxl.E-24/cm3
c    -----------------------------------
18   6   -1.19     -27 11 -18                 $ Plexi-1 starting from top
19   6   -1.19     -11 10 -25                 $ Plexi-2 conical shape
20   6   -1.19     -10 7 -19                  $ Plexi-3
21   6   -1.19     -8 7 -22 19                $ Plexi-4
22   0             -15 14 -18                 $ Sponge - neglected

1    SO   1000.0     $ Sphere for the black hole
2    SO     50.0     $ Vacuum sphere (want same order as in FLUKA)
3    SO   10.16      $ 8" sphere
4    SO    5.001     $ 10 cm lead sphere
5    SO    4.0       $ 8 cm inner PE sphere
6    PZ  -20.0       $ Bottom of scint. probe
7    PZ   -9.8       $ End PM, start plexi (cheat)
8    PZ   -9.7       $ End large plexi disc (cheat)
9    PZ   -9.512     $ End large Al tube
10   PZ   -4.051     $ Start conical transition
11   PZ   -3.670     $ End conical transition
12   PZ   -0.200     $ Bottom of LiJ crystal
13   PZ    0.200     $ Top of LiJ crystal
14   PZ    0.274     $ Top Al housing of LiJ crystal
15   PZ    0.490     $ Top of sponge above crystal
16   PZ    0.710     $ Top of Al probe housing
17   CZ    0.200     $ LiJ crystal
18   CZ    0.556     $ Inside top part of probe
19   CZ    0.655     $ Inside thicker part of probe
20   CZ    0.714     $ Out top part of probe
21   CZ    0.940     $ Outside thicker part of probe
22   CZ    1.295     $ End largest plexi
23   CZ    1.970     $ Inside PM Al housing tube
24   CZ    2.540     $ Outside PM Al housing tube
25   KZ   -1.5302424  0.06751814  -1  $ Inner cone
26   KZ   -2.4663097  0.15185759  -1  $ Outer cone
27   PZ   -0.537     $ Bottom of glass layer below LiJ
28   PX  -20.        $ Plane for the source

mode    n
imp:n   0  1 20R
m1      1001.50c 2. 6000.50c 1.       $ Polyethylene
mt1     poly.01t                      $ Poly for thermals
m2      82000.50c 1.                  $ Lead
m3      13027.50c 1.                  $ Aluminum
m4      14000.50c 1. 8016.50c 2.      $ Glass SiO2
m5      3006.50c 1.0                  $ 6- Li
m6      6012.50c 2. 1001.50c 3. 8016.50c 1.  $ C2H3O - plexi
c       GRN along x-axis
c       Uniform distribution
sdef    erg=d2 par=1 sur=28 pos=-20 0 0 rad=d1 dir=1 tme=0
si1     10.16   $ Radius of plane circular monodir. source along x-axis
sp2     -5 1.0  $ Evaporation spectrum with a=1 MeV
c  scoring
f4:n    17
fm4     0.11733  5  105   $ multiplier, material, reaction (n.alpha)
t4      200    400    600    800   1000  &
        1200   1400   1600   1800  2000  &
        2200   2400   2600   2800  3000  &
        3200   3400   3600   3800  4000  &
        4200   4400   4600   4800  5000  &
        6000   8000 10000 12000 14000 16000 18000 20000 22000 24000  &
        26000 28000 30000
c  phys:n 10.5 1.E-9 $ emax , emcnf : change emax dep. on source!!!
c  prdmp  0 500000 0 10 50000
cut:n   30000 1.0E-9
print   50 110
nps     20000000
```

77

Appendix C3

MCNP input file of the 12″ Bonner Sphere for FFTB measured neutron spectrum.

```
12" Bonner sphere with LiJ detector (no Iodine, no lead) for timing
C    JLIU 130995 (modified f-on VV/11.1.94)
1    0                1                             $ Outer void
2    0                 -1 2:-2 7 3:-2 -7 3 24:-2 -7 -23:-6 -2  $ Inner void
3    1   -0.955       -3 24 4:16 4 -3 -24        $ PE1 - outmost
4    1   -0.955       -3 -24 21 9 4 -16          $ PE2
5    1   -0.955       -5 11 20:-11 -5 26         $ PE4
6    1   -0.955       -5 16 -20                  $ PE5 - above LiJ in 5
C    ------ LEAD OR POLY LAYER --------
7    1   -0.955       -4 5 11                    $ Pb-1 upper part
8    1   -0.955       -11 -4 5 10 26             $ Pb-2 mid part with cone
9    1   -0.955       -4 -10 21                  $ Pb-3 lowest part
C    --------------------------------
10   3   -2.6989      -24 23 -9 6:-9 7 -23 22    $ AL-1 starting from bottom
11   3   -2.6989      -9 8 -22 19                $ AL-2
12   3   -2.6989      -10 9 -21 19               $ AL-3
13   3   -2.6989      -11 10 -26 25              $ AL-4 conical transition
14   3   -2.6989      -16 11 -20 18:-16 15 -18   $ AL-5 top part
-15  3   -2.6989      -14 13 -18:-13 12 -18 17   $ AL-6 around detector
C    --------------------------------
16   4   -2.2         -12 27 -18                 $ Glass
17   5    0.01655     -13 12 -17                 $ 6-Li in atx1.E-24/cm3
C    --------------------------------
18   6   -1.19        -27 11 -18                 $ Plexi-1 starting from top
19   6   -1.19        -11 10 -25                 $ Plexi-2 conical shape
20   6   -1.19        -10 7 -19                  $ Plexi-3
21   6   -1.19        -8 7 -22 19                $ Plexi-4
22   0                -15 14 -18                 $ Sponge - neglected

1    SO   1000.0      $ Sphere for the black hole
2    SO     50.0      $ Vacuum sphere (want same order as in FLUKA)
3    SO    15.24      $ 12" sphere
4    SO     5.001     $ 10 cm lead sphere
5    SO     4.0       $ 8 cm inner PE sphere
6    PZ   -20.0       $ Bottom of scint. probe
7    PZ   -10.782     $ End PM. start plexi
8    PZ   -10.465     $ End large plexi disc
9    PZ    -9.512     $ End large Al tube
10   PZ    -4.051     $ Start conical transition
11   PZ    -3.670     $ End conical transition
12   PZ    -0.200     $ Bottom of LiJ crystal
13   PZ     0.200     $ Top of LiJ crystal
14   PZ     0.274     $ Top Al housing of LiJ crystal
15   PZ     0.490     $ Top of sponge above crystal
16   PZ     0.710     $ Top of Al probe housing
17   CZ     0.200     $ LiJ crystal
18   CZ     0.556     $ Inside top part of probe
19   CZ     0.655     $ Inside thicker part of probe
20   CZ     0.714     $ Out top part of probe
21   CZ     0.940     $ Outside thicker part of probe
22   CZ     1.295     $ End largest plexi
23   CZ     1.970     $ Inside PM Al housing tube
24   CZ     2.540     $ Outside PM Al housing tube
25   KZ   -1.5302424  0.06751814  -1   $ Inner cone
26   KZ   -2.4663097  0.35185759  -1   $ Outer cone
27   PZ    -0.537     $ Bottom of glass layer below LiJ
28   PX   -20.        $ Plane for the source

mode    n
imp:n   0  1 20R
m1      1001.50c 2. 6000.50c 1.        $ Polyethylene
mt1     poly.01t                       $ Poly for thermals
m2      82000.50c 1.                   $ Lead
m3      13027.50c 1.                   $ Aluminum
m4      14000.50c 1. 8016.50c 2.       $ Glass SiO2
m5      3006.50c 1.0                   $ 6- Li
m6      6012.50c 2. 1001.50c 3. 8016.50c 1. $ C2H3O - plexi
c       FFTB spectrum along x-axis
c       Uniform distribution
sdef    erg=d1 par=1 sur=28 pos=-20 0 0 rad=d2 dir=1 tme=0
si1           0  0.000000414  0.0000006826  0.000001445  0.000003059 &
        0.000006476  0.00001371  0.00002902  0.00006144  0.0001301 &
        0.0002754  0.0005929  0.001234  0.002613  0.005531 &
        0.01171  0.02479  0.05247  0.1111  0.2237 &
        0.4508  0.9072  1.872  3.679  7.408 &
        14.92  20.0
sp1  c        0  108000  116124  126794  136239 &
        144998  153349  161496  169655  177999 &
        186716  196147  205821  216541  228281 &
        241361  256131  273241  294101  319331 &
        353621  398511  454501  505971  554621 &
        600031  618431
si2     15.24   $ Radius of plane circular monodir. source along x-axis
c       scoring
f4:n    17
fm4     0.11733  5  105   $ multipler. material. reaction (n,t)
t4      200  1000  2000  3000  4000 &
        5000  6000  7000  8000  9000  10000 &
        12000  14000  16000  18000  20000  24000  28000 &
        32000  36000  40000
c phys:n 10.5  1.E-9   $ emax . emcnf : change emax dep. on source!!!
c prdmp  0 500000 0 10 50000
cut:n   40000 1.0E-9
print   50 110
nps     80000000
```

78

Appendix D

A portion of MCNP output file of moderated BF_3 detector for 1 MeV neutrons.

```
1tally    4        nps =  1000000
            tally type 4    track length estimate of particle flux.
            tally for  neutrons

            volumes
                 cell:       1
                      6.08684E+02

cell  1
multiplier bin:  -2.40000E-01    1        107
        time:      1.0000E+03          2.0000E+03          3.0000E+03          4.0000E+03          5.0000E+03
                 9.35310E-07  .0061   9.55932E-07  .0074   9.76424E-07  .0074   9.79456E-07  .0073   9.50518E-07  .0072

        time:      6.0000E+03          7.0000E+03          8.0000E+03          9.0000E+03          1.0000E+04
                 9.06236E-07  .0073   8.41001E-07  .0074   7.83048E-07  .0075   7.21384E-07  .0077   6.64107E-07  .0078

        time:      1.1000E+04          1.2000E+04          1.3000E+04          1.4000E+04          1.5000E+04
                 6.15358E-07  .0080   5.64408E-07  .0081   5.17702E-07  .0083   4.75776E-07  .0085   4.30377E-07  .0087

        time:      1.6000E+04          1.7000E+04          1.8000E+04          1.9000E+04          2.0000E+04
                 3.84127E-07  .0089   3.51946E-07  .0091   3.21406E-07  .0093   2.91359E-07  .0096   2.59913E-07  .0099

        time:      2.1000E+04          2.2000E+04          2.3000E+04          2.4000E+04          2.5000E+04
                 2.33898E-07  .0102   2.11403E-07  .0105   1.89400E-07  .0108   1.73000E-07  .0113   1.57311E-07  .0119

        time:      2.6000E+04          2.7000E+04          2.8000E+04          2.9000E+04          3.0000E+04
                 1.41351E-07  .0126   1.28167E-07  .0133   1.16527E-07  .0141   1.03600E-07  .0149   9.14110E-08  .0158

        time:      3.1000E+04          3.2000E+04          3.3000E+04          3.4000E+04          3.5000E+04
                 8.240:5E-08  .0165   7.52893E-08  .0171   6.84413E-08  .0179   6.01849E-08  .0188   5.42317E-08  .0197

        time:      3.6000E+04          3.7000E+04          3.8000E+04          3.9000E+04          4.0000E+04
                 4.762S7E-08  .0211   4.17395E-08  .0226   3.88739E-08  .0237   3.44277E-08  .0252   3.07880E-08  .0268

        time:      4.1000E+04          4.2000E+04          4.3000E+04          4.4000E+04          4.5000E+04
                 2.82520E-08  .0282   2.56677E-08  .0295   2.23829E-08  .0315   1.97588E-08  .0334   1.83044E-08  .0343

        time:      4.6000E+04          4.7000E+04          4.8000E+04          4.9000E+04          5.0000E+04
                 1.62399E-08  .0363   1.49800E-08  .0378   1.36809E-08  .0393   1.27901E-08  .0408   1.16688E-08  .0437

        time:       total
                 1.51896E-05  .0042
1status of the statistical checks used to form confidence intervals for the mean for each tally bin


tally    result of statistical checks for the tfc bin (the first check not passed is listed) and error magnitude check for all bins

    4    passed the 10 statistical checks for the tally fluctuation chart bin result
         passed all bin error check:     51 tally bins all have relative errors less than  .10 with no zero bins


the 10 statistical checks are only for the tally fluctuation chart bin and do not apply to other tally bins.
```

79

Appendix E

MCNP Calculations of response of BF$_3$ detector and Anderson-Braun remmeter.

Energy	BF$_3$ detector (822 cm^2)[a]			AB remmeter (490 cm^2)[a]		
	Counts [b]	Error (%)	Response [c] [cm^2]	Counts [b]	Error (%)	Response [c] [cm^2]
0.1 eV	—	—	—	—	—	—
0.6 eV	2.71E-06	0.87	2.23E-03	—	—	—
1 eV	4.00E-06	0.72	3.29E-03	—	—	—
10 eV	5.92E-06	0.80	4.86E-03	2.62E-08	5.70	1.31E-05
100 eV	6.11E-06	0.61	5.02E-03	—	—	—
1 keV	8.08E-06	0.55	6.64E-03	1.41E-07	2.90	7.02E-05
10 keV	8.79E-06	0.53	7.22E-03	—	—	—
100 keV	1.02E-05	0.50	8.35E-03	7.85E-07	0.92	3.91E-04
500 keV	1.39E-05	0.44	1.15E-03	2.94E-06	0.67	1.47E-03
750 keV	1.48E-05	0.42	1.22E-03	—	—	—
1 MeV	1.52E-05	0.42	1.22E-03	4.59E-06	0.54	2.29E-03
2 MeV	1.40E-05	0.44	1.15E-03	5.63E-06	0.49	1.55E-03
10 MeV	—	—	—	3.12E-06	0.64	1.55E-03
20 MeV	4.07E-06	0.81	3.35E-03	—	—	—
GRN	1.33E-05	0.45	1.09E-02	4.72E-06	0.37	2.35E-03
FFTB	8.14E-06	0.57	6.69E-03	2.03E-06	0.80	1.01E-03

[a] cross sectional area of the detector

[b] number of reactions per source neutron in LiI

[c] per unit fluence